JCB Journal of Cell Biology

ARTICLE

EGFR-mediated epidermal stem cell motility drives skin regeneration through COL17A1 proteolysis

Daisuke Nanba[1], Fujio Toki[1], Kyosuke Asakawa[1], Hiroyuki Matsumura[1], Ken Shiraishi[2], Koji Sayama[2], Kyoichi Matsuzaki[3], Hiroshi Toki[4,5], and Emi K. Nishimura[1,6]

Skin regenerative capacity declines with age, but the underlying mechanisms are largely unknown. Here we demonstrate a functional link between epidermal growth factor receptor (EGFR) signaling and type XVII collagen (COL17A1) proteolysis on age-associated alteration of keratinocyte stem cell dynamics in skin regeneration. Live-imaging and computer simulation experiments predicted that human keratinocyte stem cell motility is coupled with self-renewal and epidermal regeneration. Receptor tyrosine kinase array identified the age-associated decline of EGFR signaling in mouse skin wound healing. Culture experiments proved that EGFR activation drives human keratinocyte stem cell motility with increase of COL17A1 by inhibiting its proteolysis through the secretion of tissue inhibitor of metalloproteinases 1 (TIMP1). Intriguingly, COL17A1 directly regulated keratinocyte stem cell motility and collective cell migration by coordinating actin and keratin filament networks. We conclude that EGFR-COL17A1 axis–mediated keratinocyte stem cell motility drives epidermal regeneration, which provides a novel therapeutic approach for age-associated impaired skin regeneration.

Introduction

Aging is characterized by a time-dependent decline in the homeostatic functions of most tissues and organs (López-Otín et al., 2013). In mammals, including humans, aging impairs the skin's regenerative capacity after injury (Ashcroft et al., 2002; Kim et al., 2015; Sgonc and Gruber, 2013). This age-associated impaired skin wound healing predisposes patients to nonhealing chronic disorders that are recognized as age-related complications, including diabetic ulcers, pressure sores, and venous stasis ulcers (Eming et al., 2014). Skin wound healing results from collaborative behaviors of many different types of cells and occurs in several overlapping but distinct stages: hemostasis, inflammation, proliferation, and remodeling (Gurtner et al., 2008; Sun et al., 2014). Although aging is assumed to affect all stages of wound healing processes (Sgonc and Gruber, 2013), clinical experiments using healthy human volunteers have demonstrated that aging leads to delayed reepithelialization in the proliferation stage (Holt et al., 1992).

Reepithelialization is an essential process for completion of the skin wound closure. During reepithelialization, keratinocytes migrate over the injured dermis and close the epithelial gap while restoring barrier function. It has been demonstrated that after injury, the epidermis is organized into two distinct compartments surrounding the wound: a leading edge consisting of migratory nonproliferative cells at the front and a stationary zone of proliferative cells at the back (Aragona et al., 2017; Coulombe, 2003; Usui et al., 2005). Recently, live imaging of mouse skin wound healing has revealed that these two compartments spatially overlap to some extent and that migratory proliferating cells exist between those compartments (Park et al., 2017), which suggests that the migratory and proliferative capacities of keratinocytes are not exclusive and are highly coordinated during reepithelialization. However, the coordination of cell division and migration of these stem cells during reepithelialization remains unknown.

Human epidermal keratinocyte stem cells give rise to progressively growing colonies (Barrandon and Green, 1987b; Rheinwald and Green, 1975). A single keratinocyte stem cell produces plenty of progeny by multiple cell divisions and creates a large multilayered colony, which enables ex vivo production of epidermal sheets for skin regenerative medicine (Hynds et al., 2018; Nanba, 2019). Exponential growth of the keratinocyte colony is achieved by the coordination of cell proliferation and

[1]Department of Stem Cell Biology, Medical Research Institute, Tokyo Medical and Dental University, Tokyo, Japan; [2]Department of Dermatology, Ehime University School of Medicine, Toon, Japan; [3]Department of Plastic and Reconstructive Surgery, International University of Health and Welfare, School of Medicine, Narita, Japan; [4]Research Center for Nuclear Physics, Osaka University, Osaka, Japan; [5]Health Care Division, Health and Counseling Center, Osaka University, Osaka, Japan; [6]Division of Aging and Regeneration, Institute of Medical Science, The University of Tokyo, Tokyo, Japan.

Correspondence to Daisuke Nanba: nanbscm@tmd.ac.jp; Emi K. Nishimura: emikn@g.ecc.u-tokyo.ac.jp.

migration (Barrandon and Green, 1987a; Nanba et al., 2013b; Nanba et al., 2015) and shows a phenotypic similarity to the collective migration of keratinocytes from human skin fragments, which is assumed to reproduce reepithelialization ex vivo (Fig. 1 A). This collective migration of keratinocytes from the skin fragments was impaired when the skin was isolated from the affected foot skin of a patient with critical limb ischemia (CLI) and a diabetic background but not from the unaffected trunk skin (Fig. 1 B), as was also seen in skin fragments isolated from obese (ob/ob) mice (Mazzalupo et al., 2002) and aged mice (Keyes et al., 2016). Thus, the growth of the human keratinocyte colony is a suitable experimental model for elucidating the precise molecular and cellular mechanisms of reepithelialization in human skin. In this study, we dissect human keratinocyte stem cell dynamics in colony expansion and reveal that growth factor signaling–mediated motility of keratinocyte stem cells is essential for reepithelialization.

Results

Human keratinocyte cultures contain expanding and stacking colonies

Human keratinocytes give rise to several types of colonies, including progressively growing, terminal (abortive), and mixed colonies (Fig. S1 A; Rochat et al., 2012). Progressively growing colonies, also called "expanding" colonies (Roshan et al., 2016), have a circular shape and consist of densely packed small basal cells with involucrin (IVL)-expressing stratified cells (Fig. 1 C and Fig. S1, A and B). Human keratinocyte cultures also contain colonies that show stacking of IVL-positive cells on the basal cells (Fig. 1 C). This colony type, named a "stacking" colony, has an irregular stratified structure with a cluster of differentiated keratinocytes at its center (Fig. S1 B). While the formation of both expanding and stacking colonies is required for several rounds of cell division, clonal analysis revealed that stacking colonies are initiated from transient amplifying keratinocytes and that expanding colonies are initiated mainly from keratinocyte stem cells and progenitor cells (Fig. S1 C). As the expanding and stacking phenotypes of the colonies have phenotypic similarities to the progressive and impaired collective migration of keratinocytes, we analyzed the spatiotemporal dynamics of human keratinocytes during the formation of expanding and stacking colonies.

Lineage analysis of keratinocytes in the formation of expanding and stacking colonies

Time-lapse imaging of human keratinocyte colonies containing several cells was performed until the small colonies grew into expanding or stacking colonies (Fig. 1 D), and the lineage trees of keratinocytes during the colony formation were reconstructed, as previously described (Dover and Potten, 1988; Roshan et al., 2016). The lineage analysis revealed that some keratinocytes continuously divide and form expanding colonies (Fig. 1 E), while other keratinocytes gradually arrest the cell cycle and form stacking colonies (Fig. 1 F). According to the classification by Roshan et al. (2016), we also analyzed cell fate determination during the formation of expanding and stacking colonies (Fig. 1 G and Materials and methods). Most (97.9%) of the cell divisions in the expanding colony formation were proliferating/proliferating (PP) divisions. In the stacking colony formation, however, 53.3% of all divisions were differentiating/differentiating (DD) divisions, and PP divisions were markedly decreased (34.7%; Fig. 1 H). Cell fate analysis in the first three rounds of cell division revealed that PP division was predominant throughout expanding colony formation (Fig. 1 H). Although PP division (68.1%) was also predominant in the first round of cell division in the stacking colony formation, PP division continuously decreased. Conversely, DD division increased along with the stacking colony formation and reached 77.1% of all divisions in the third round of cell division (Fig. 1 H).

We then measured cell cycle entry and cell cycle duration during the formation of both types of colonies. The ratio of keratinocytes with active DNA synthesis labeled with 5-ethynyl-2′-deoxyuride (EdU) in expanding colonies was higher than that in stacking colonies (Fig. 1 I). However, there was not much difference in the median cell cycle length between expanding (13.8 h) and stacking (14.4 h) colony-forming keratinocytes (Fig. 1 J and Fig. S1 D). These results indicate that keratinocytes forming stacking colonies become quiescent without an extension of the cell cycle duration.

Keratinocytes with higher locomotive ability give rise to expanding colonies

Next, we analyzed cell locomotion in colonies. Expanding colony-forming keratinocytes changed their positions, but stacking colony-forming keratinocytes were highly stable on culture day 2 (Fig. 2 A). We measured the cell locomotion speed of keratinocytes during colony formation, and the motion analysis confirmed that keratinocytes forming expanding colonies move faster than those forming stacking colonies on culture days 2 and 3 (Fig. 2 B).

Cell motion analysis also revealed heterogeneity of the cell locomotion speed among keratinocytes during expanding colony formation. We further analyzed the fate of locomotive and stationary cells on culture day 2 using lineage tracing (Fig. 2 C) and found that the more-locomotive cells also generate more descendants than the less-locomotive cells during expanding colony formation (Fig. 2 D). This result strongly suggests that cell locomotive ability is correlated with cell proliferative ability, even in the single colony formation.

We examined cell division orientation during the formation of human keratinocyte colonies. Keratinocytes in small non-stratified colonies (culture day 4), expanding and stacking colonies (culture day 6), and confluent epidermal sheets (culture day 15) were fixed and analyzed by confocal microscopy. 3D reconstructions revealed that keratinocytes became taller before cell division and overlaid their neighboring cells (Figs. 2 E and S2 A). During cell division, keratinocytes attached to the substrate surface (Fig. 2 E), but cells dividing over other basal keratinocytes were also observed (Fig. S2 A). We then examined the spindle orientation in mitosis by visualizing microtubules and nuclei (Fig. S2 B) and found that most keratinocytes divided horizontally in this culture condition, even in the formation of stacking colonies and stratified sheets (Fig. 2 E).

We next focused on keratinocyte behavior after cell division. We found that two daughter cells exhibited two modes of behavior

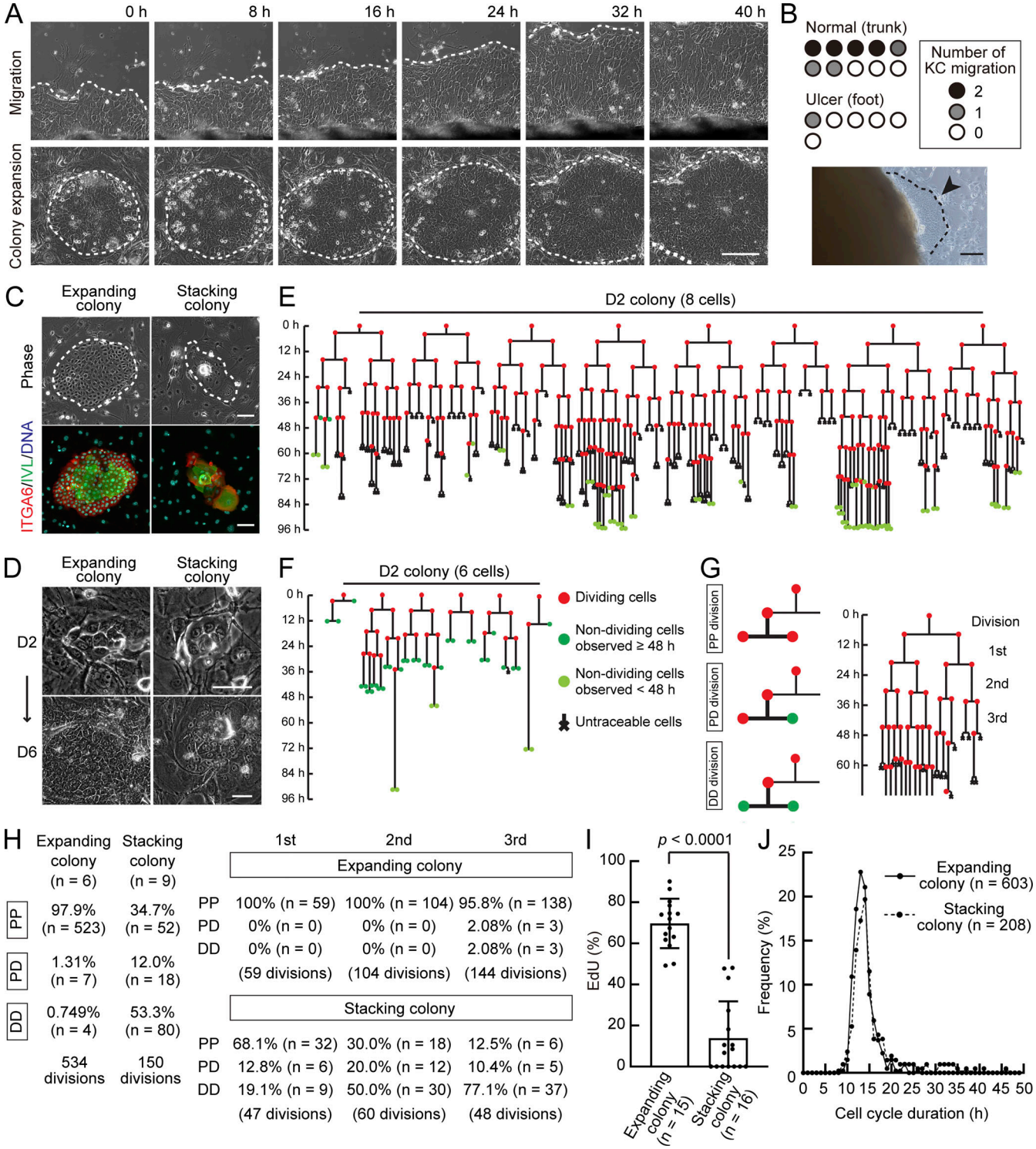

Figure 1. **Single-cell lineage tracing during the formation of human keratinocyte colonies. (A)** Similarity of keratinocyte migration from human skin fragments (upper) and human keratinocyte colony expansion (lower). White dotted lines indicate the periphery of migrating keratinocytes and expanding keratinocyte colonies. Scale bar, 200 µm. **(B)** Number of keratinocyte (KC) migration from skin fragments isolated from trunk and foot ulcer regions of a single patient with CLI within 3 wk of culture. Black arrowhead and dotted line indicate the area and periphery of migrating keratinocytes, respectively. Scale bar, 500 µm. **(C)** Appearance of expanding and stacking colonies of human epidermal keratinocytes 6 d after inoculation. White dotted lines indicate the periphery of keratinocyte colonies. Scale bars, 100 µm. **(D)** Experimental design of tracing the formation of expanding and stacking colony growth at single-cell resolution. Serial images were obtained at 5-min intervals on culture days 2 to 6. Scale bars, 50 µm. **(E and F)** Representative images of lineage tracing of expanding (E) and stacking (F) colonies. **(G)** Classification of PP, PD, and DD divisions, and orders of cell divisions during this experimental condition. **(H)** Cell fate determination during expanding and stacking colony formation. **(I)** Frequency (mean ± SD) of EdU-incorporated cells in expanding and stacking colonies on culture day 6. Colonies were treated with EdU for 24 h before fixation. **(J)** Distribution of cell cycle duration during expanding and stacking colony formation.

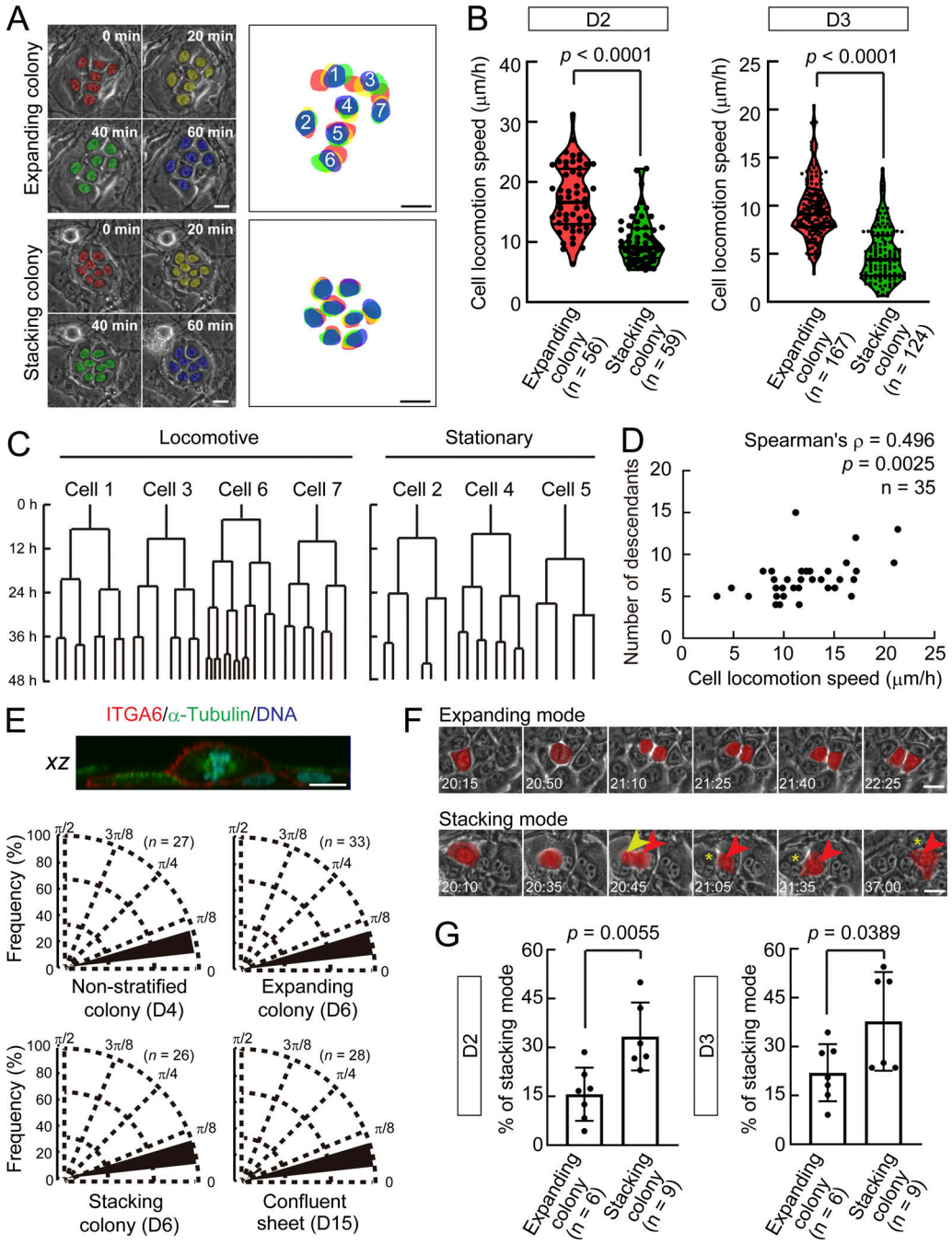

Figure 2. **Keratinocyte motility is coupled with colony expansion. (A)** Motion of individual keratinocytes forming expanding and stacking colonies on culture day 2. Nuclei are labeled with pseudo-colors at 10-min intervals. Scale bars, 20 μm. **(B)** Distribution of locomotion speed of cells forming in expanding and stacking colonies on culture days 2 (left) and 3 (right). The values were obtained from 2-h observations each day. **(C)** Lineage tracing of cells forming the expanding colony on culture days 2–4 represented in Fig. 2 A. Locomotive (cells 1, 3, 6, and 7) and stationary (cells 2, 4, and 5) cells were analyzed. **(D)** Correlation between cell locomotion speed and the proliferative capacity of keratinocytes in expanding colonies. **(E)** Distribution of cell division angles during keratinocyte colony and sheet formation. Upper image shows a representative vertical (*x*–*z*) section of a dividing keratinocyte during colony formation. Scale bar, 10 μm. **(F)** Representative images of expanding and stacking modes after cell division. Nuclei are labeled with a pseudo-color (red). The yellow arrowhead indicates one dividing nucleus. A daughter cell containing this nucleus resides at the basal layer (yellow asterisks). Red arrowheads indicate another daughter cell that remains in the suprabasal layer after cell division. Scale bars, 20 μm. **(G)** Frequency of stacking mode after cell division during the formation of expanding and stacking colonies on culture days 2 (left) and 3 (right). The values (mean ± SD) were obtained from 24-h observations of the formation of each colony. P values were calculated with the two-tailed Mann–Whitney *U* test in B and G.

after cell division in the colony. Two daughter cells produced by planar cell division remained in the basal layer and expanded the colony (Figs. 2 F and S2 C). We termed this behavior the "expanding" mode of cell division. Human keratinocytes also exhibited another mode of behavior after cell division. Planar cell division occurred on the basal layer, and one or two daughter cells remained at the suprabasal layer (Figs. 2 F and S2 D), became large, and flattened on the basal layer. This mode of keratinocyte behavior was termed the "stacking" mode. The vertical movements of keratinocytes in the stacking mode were confirmed by confocal microscopy, with keratinocytes expressing nuclear-targeted GFP and plasma membrane–targeted mCherry (Fig. S2 E). We analyzed 227 and 281 cell divisions on culture days 2 and 3, respectively, and found that the frequency of the stacking mode was significantly higher in stacking colony-forming keratinocytes than in expanding colony-forming keratinocytes (Fig. 2 G). If basal cells move faster in the colony, suprabasal cells can find space to settle down in the basal layer and reside there. Therefore, we assumed that the decrease in cell motility results in an increase in the stacking mode after cell division and the stacking colony phenotype.

Cell kinetic model predicts that keratinocyte motility is essential for sustained growth of colonies

We previously reported a unique rotational motion of two-cell colonies of human keratinocytes, and our simulation experiments revealed that the rotational motion of individual keratinocytes generates cell locomotion in the colony (Nanba et al., 2015). In this study, as image analysis suggested that differences in cell locomotion ability are involved in the generation of expanding and stacking colony phenotypes, we hypothesized that differences in the rotational speed of individual keratinocytes result in the differences in colony phenotypes between expanding and stacking colonies. To test this idea, we modeled keratinocyte colony formation based on our observations (Fig. S3, described in Materials and methods) and performed simulation experiments to investigate whether expanding and stacking colonies can be generated if only the cell rotational speed is modified, since we cannot modulate cell motility without affecting cell proliferative activity in cell culture experiments.

A single cell was cultivated for 6 d in silico, and the numerical calculations demonstrated that cell production was proportional to the rotational speed of cells up to 0.6 π/h of rotational speed (Fig. 3 A) and basal cells could be efficiently expanded when cells were given 0.4–0.7 π/h of rotational speed (Fig. 3 B). Cell locomotion speed in the colony was dependent on the rotational speed of cells (Fig. 3 C). We next examined colony growth from single keratinocytes with three different rotational speeds (0, 0.1, and 0.5 π/h). The numerical calculations and 2D visualization of colonies clearly revealed that the rotational speed is essential for the exponential growth of colonies (Fig. 3, D and E). The 3D structure of colonies was also reconstructed in silico (Fig. 3 F). If cells had no rotational ability, the colony did not grow and had many stratified layers. However, when cells were given rotational ability, the colonies grew remarkably and contained a smaller number of stratified cells. These simulation experiments reproduced the expanding and stacking colony phenotypes (Fig. 3 G) by modulating only the rotational speed of cells.

When a number of keratinocyte stem cells are seeded into a cell culture dish at optimal density, the resulting keratinocyte colonies fuse with each other and form functional stratified keratinocyte sheets (Banks-Schlegel and Green, 1980; Green et al., 1979). Our simulation program can also set the area for colony growth, and we reproduced a confluent cell culture to generate the keratinocyte sheet in silico. When an individual keratinocyte was provided with an area with a 100-μm radius for colony growth, numerical calculations revealed that the rotational motion of keratinocytes increased the number of keratinocytes in each layer of the stratified colony (Fig. 3, H and I). Furthermore, 3D reconstruction of colony growth clearly indicated that rotational activity is required for the generation of uniform stratified keratinocyte sheets (Fig. 3 J). These simulation experiments also indicate that the rotational motion of keratinocytes is required for epidermal regeneration.

Decline of EGF receptor (EGFR) signaling in skin wound healing with aging

Our live-imaging and simulation experiments indicated that the motility of keratinocytes is associated with colony expansion and stemness. A variety of intracellular signaling mediated by receptor tyrosine kinases (RTKs) is indispensable for keratinocyte migration and reepithelialization (Gurtner et al., 2008), suggesting that changes in RTK signaling are related to age-associated impaired wound healing by modulating keratinocyte motility. To identify age-associated changes in RTK signaling during wound healing, we prepared tissue lysates from wounds in the dorsal skin of young (12-wk-old) and aged (19–25-mo-old) mice, 3 d after wounding (Figs. 4 A and S4 A), and the obtained lysates were then subjected to a phospho-RTK array to identify RTK signaling that is altered during aging. Strong signals of phospho-EGFR and phospho-ErbB2 were detected in the protein lysate prepared from the wound in the young mice, but the signals of these two RTKs were decreased in the lysates from the aged mice (Fig. S4, C and D). Western blot analysis confirmed these results and also revealed that the level of phosphorylated EGFR was reduced in protein lysates prepared from aged mice, even though the EGFR expression level was maintained (Fig. 4 B). Decline of phosphorylated ErbB2 was associated with decreased expression of ErbB2 (Fig. 4 B). A few other strong signals of phosphorylated RTKs were also observed in the wounded skin, but these signals were not altered during aging (Fig. S4, C and D). EGFR was mainly expressed in the basal layer of the epidermis, and EGFR expression and its phosphorylation levels in the normal skin of aged mice were similar to those of young mice (Fig. S4 E).

Wound healing experiments strongly suggested that the decline of EGFR signaling with aging results in an age-associated alteration of keratinocyte migration and reepithelialization in humans. The decreased phosphorylation of EGFR results from the reduced production of EGFR ligands in wounds and/or the dysregulation of EGFR signaling in keratinocytes. We next examined whether the decreased EGFR activation in the wounded skin of aged keratinocytes is due to an intrinsic or extrinsic effect, using human keratinocytes isolated from infants (5–19-mo-old) and from aged (70–78-yr-old) patients. Recombinant human EGF induced EGFR phosphorylation and internalization

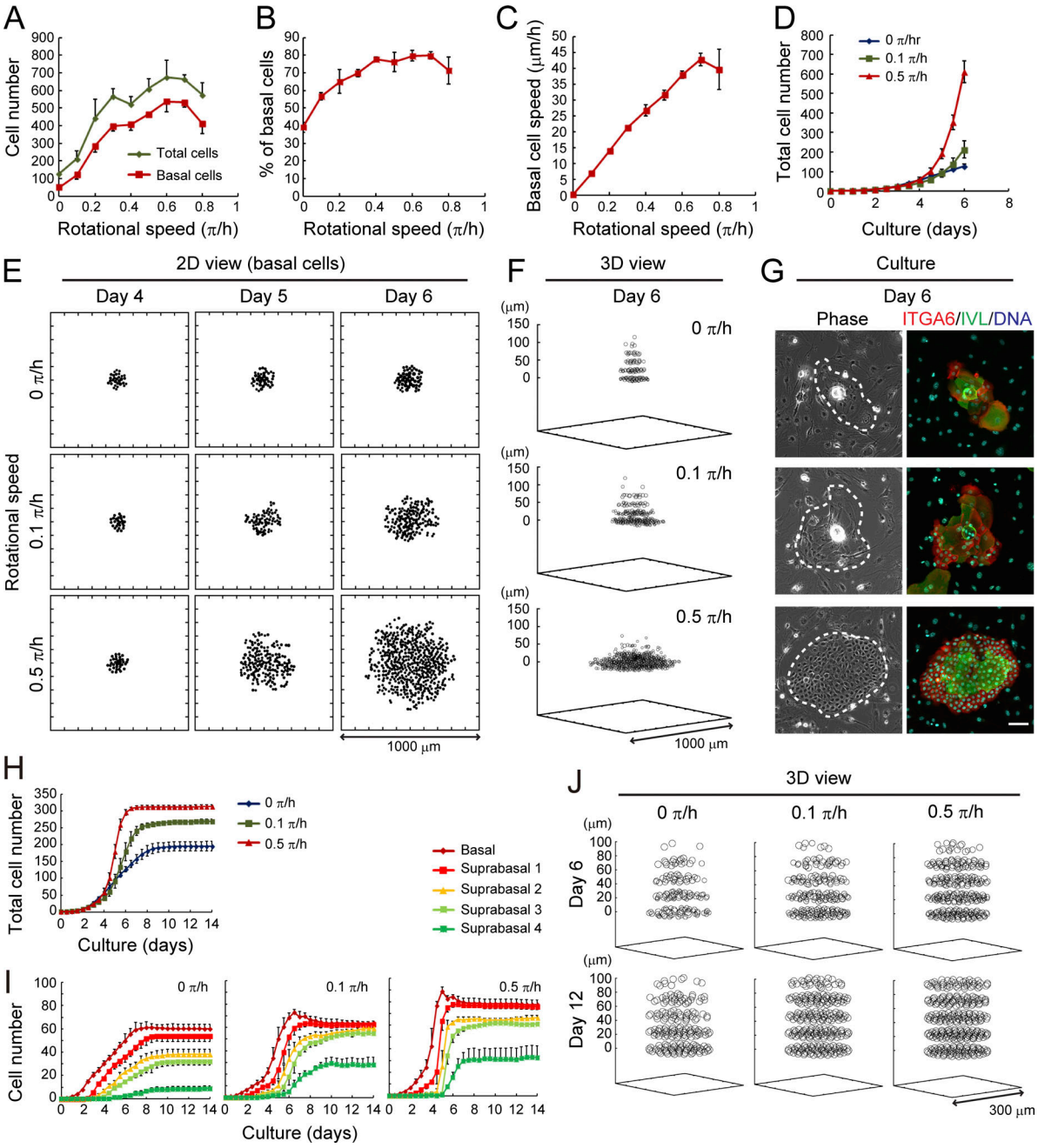

Figure 3. **In silico reconstitution of keratinocyte colony growth predicts that keratinocyte motility is essential for epidermal regeneration. (A)** The number of total and basal keratinocytes with various rotational speeds of cells on culture day 6. **(B)** The ratio of basal keratinocytes to total cells in the colony with various rotational speeds on culture day 6. **(C)** Average speed of basal keratinocytes with various rotational speeds on culture day 6. **(D)** The total number of cells in keratinocyte colonies consisting of cells with 0, 0.1, or 0.5 π/h rotational speed during 6 d of cultivation. **(E)** 2D images of keratinocyte colony growth with three types of rotational speeds of cells. **(F)** 3D images of keratinocyte colonies with three types of rotational speeds of cells on culture day 6. **(G)** Representative images of cultured human keratinocyte colonies with three types of morphologies on culture day 6 (also shown in Fig. 1 C). White dotted lines indicate the periphery of keratinocyte colonies. Scale bar, 100 μm. **(H–J)** Cells grew within a limited area with a 100-μm radius to simulate high-density cell cultures. **(H)** The total number of cells in keratinocyte sheets consisting of cells with 0, 0.1, or 0.5 πr/h rotational speed during 14 d of cultivation. **(I)** Number of cells in the basal and the upper suprabasal layers of keratinocyte sheets with three types of rotational speeds of cells during 14 d of cultivation. **(J)** 3D images of keratinocyte sheets with three types of rotational speeds of cells on culture days 6 (upper) and 12 (lower). The values reported (mean ± SD) were obtained from calculations using a random number generator with five random seeds in A–D, H, and I.

of EGFR in keratinocytes isolated from both infants and aged patients (Figs. 4 C and S4 F). Furthermore, the EGF-induced expansion of keratinocyte colonies (Barrandon and Green, 1987a; Nanba et al., 2013b) was not impaired in keratinocytes isolated from aged patients (Fig. 4, D and E). The addition of EGF also increased the formation of expanding colonies in cultures of both types of keratinocytes (Fig. 4 F). Collectively, these results strongly suggested that a cell-extrinsic defect of

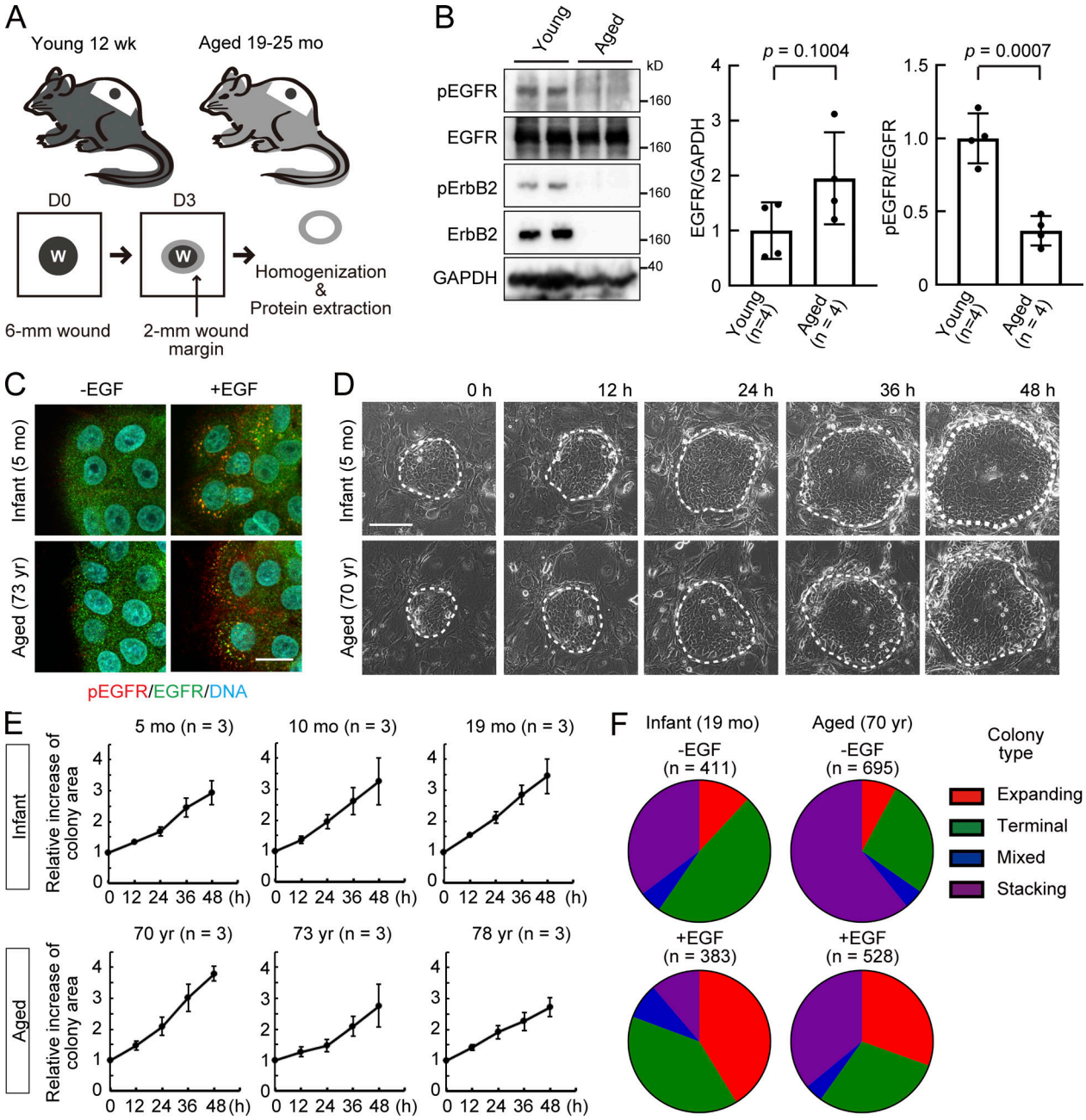

Figure 4. **Age-associated decline of EGFR signaling in wound healing. (A)** Schematic representation of wound healing experiments with young and aged mice. Details are described in Materials and methods. **(B)** Left: Western blots of EGFR, phosphorylated EGFR (pEGFR), ErbB2, and phosphorylated ErbB2 (pErbB2). Middle and right: Quantification of EGFR and pEGFR expression normalized by GAPDH and EGFR, respectively. **(C)** Immunostaining with anti-EGFR and anti-pEGFR in infant and aged human keratinocytes with or without EGF treatment. Scale bar, 20 µm. **(D)** EGF-induced colony expansion of infant and aged human keratinocytes. White dotted lines indicate the periphery of keratinocyte colonies. Scale bar, 200 µm. **(E)** Relative increase in area of expanding colonies of keratinocytes isolated from infants and aged patients after the addition of EGF. **(F)** Distribution of colony types after 6 d of cultivation with or without EGF in cultures of infant and aged keratinocytes. The ages of patients from whom keratinocytes were isolated are indicated in each graph. P values were calculated with the two-tailed Student's *t* test

EGFR activation causes the delayed skin wound healing associated with aging.

EGFR signaling accelerates keratinocyte stem cell motility and epidermal regeneration

We next investigated how EGFR activation alters human keratinocyte behaviors by using neonatal keratinocytes. The addition of EGF enhanced the rotational speed of two-cell colonies of keratinocytes (Fig. 5 A). In particular, EGF was required for the maintenance of a two-cell colony population with higher rotational speed (≥0.5 π/h) that showed significant proliferative capacity (Nanba et al., 2015), indicating that EGFR signaling is involved in keratinocyte stem cell motility. Treatment with EGF also increased the cell locomotion speed of individual

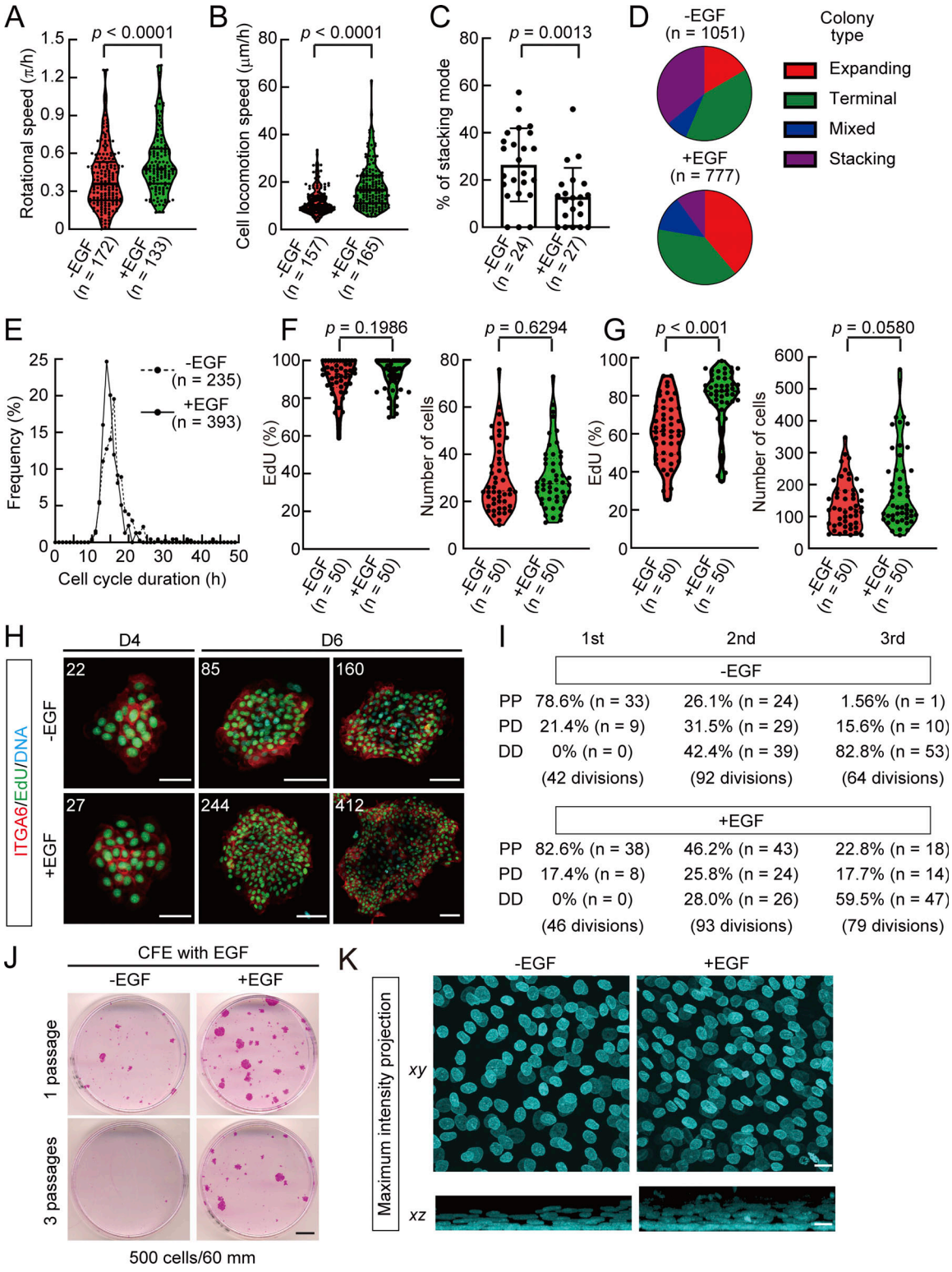

Figure 5. **EGFR activation is required for keratinocyte stem cell motility and epidermal regeneration. (A)** Distribution of rotational speed of two-cell colonies of human keratinocytes with and without EGF on culture day 1. **(B)** Distribution of locomotion speed of individual cells in human keratinocyte colonies with and without EGF in culture day 2. **(C)** Frequency of stacking mode after cell division during keratinocyte colony formation with and without EGF. The values (mean ± SD) were obtained from 48-h observation on culture days 2–4. **(D)** Distribution of keratinocyte colony types after 6 d of cultivation with and without EGF. **(E)** Distribution of cell cycle duration during keratinocyte colony formation with and without EGF. **(F and G)** Frequency of EdU-incorporated cells (left) and distribution of cell numbers (right) in keratinocyte colonies on culture days 4 (F) and 6 (G) with or without EGF. **(H)** Localization of EdU-incorporated cells in keratinocyte colonies on culture days 4 and 6 with or without EGF. Scale bars, 50 μm (left) and 200 μm (middle and right). **(I)** Cell fate determination during colony formation with or without EGF. **(J)** Colony-forming efficiency of human keratinocytes after serial cultivation with and without EGF. Scale bar, 10 mm. **(K)** Keratinocyte sheet formation with and without EGF. Upper and lower panels show the *x*–*y* and *x*–*z* maximum-intensity projections, respectively. Scale bars, 20 μm. P values were calculated with the two-tailed Mann–Whitney *U* test in A–C, F, and G.

keratinocytes in the colony (Fig. 5 B). Furthermore, treatment of human keratinocytes with EGF decreased the stacking mode after cell division (Fig. 5 C) and the generation of stacking colonies (Fig. 5 D). Thus, these cell culture experiments confirmed that the rotational speed was correlated with the mean speed of cell locomotion in the colony and keratinocyte colony phenotypes, as predicted from simulation experiments (Fig. 3). Treatment with EGF did not shorten the cell cycle duration of human keratinocytes (Figs. 5 E and S1 E) and did not enhance cell proliferation until culture day 4 (Fig. 5 F). However, treatment with EGF significantly increased the ratio of proliferative cells in the colony at culture day 6 (Fig. 5 G) by stimulating keratinocytes located at both the central and peripheral regions of the colony (Fig. 5 H). Lineage tracing analysis also revealed that treatment with EGF prevented the rapid decline of PP divisions in the culture (Fig. 5 I), which also confirmed that the addition of EGF to the culture medium is required for the long-term maintenance of human keratinocyte stem cells ex vivo (Fig. 5 J). These results indicate that EGF maintains the properties of human keratinocyte stem cells, including both their self-renewal and higher locomotive phenotypes.

As noted above, simulation experiments predicted that keratinocyte stem cell motility is required for epidermal sheet formation (Fig. 3, H–J). These results were also confirmed by cell culture experiments. Confluent keratinocyte cultures without EGF contained a smaller number of cells and exhibited less stratification than those cultured with EGF (Fig. 5 K). However, keratinocyte cultures containing EGF did produce the uniform stratified keratinocyte sheets (Fig. 5 K). Thus, EGFR activation is also required for the generation of epidermal tissues ex vivo.

EGFR signaling inhibits COL17A1 proteolysis by inducing TIMP1 secretion

We have previously demonstrated that hemidesmosomal components are crucial for the motility and maintenance of human keratinocyte stem cells (Liu et al., 2019; Nanba et al., 2015). We next investigated whether EGFR activation changes the expression of hemidesmosomal proteins and found that levels of collagen XVII (COL17A1), a transmembrane component of hemidesmosomes, were increased after EGF treatment (Fig. 6, A and B). Levels of COL17A1 were increased during the 24 h after EGF stimulation, and the enhanced expression of COL17A1 was maintained for at least the next 24 h (Fig. S5 A). COL17A1 levels were decreased when keratinocytes were treated with the EGFR inhibitor PD168393 (Fig. 6 C) and with the MEK inhibitor PD98059 (Fig. S5 B), which indicated that the EGFR-ERK MAPK pathway regulates COL17A1 expression. However, quantitative PCR analysis revealed that *COL17A1* mRNA levels were not increased after EGFR activation (Figs. 6 D and S5 D). As COL17A undergoes posttranscriptional regulation by proteolytic enzymes (Hirako and Owaribe, 1998; Nishie, 2020), we investigated the mRNA expression levels of several proteases and protease inhibitors that are associated with COL17A1 proteolysis (Fig. S5 C; Franzke et al., 2009; Franzke et al., 2002; Hofmann et al., 2009; Laval et al., 2014; Lin et al., 2012; Liu et al., 2000; Nishimura et al., 2016; Ståhle-Bäckdahl et al., 1994; Verraes et al., 2001). While altered mRNA expression levels of proteases, including *ADAM9*, *10*, *17*, and *ELANE*, were not observed, the level of *MMP9* mRNA was significantly increased by EGFR activation (Fig. S5 D). Intriguingly, levels of several types of protease inhibitors, including *PAI-1* (*SERPINE1*), *PAI-2* (*SERPINB2*), *A1AT*, and *TIMP1*, were increased after EGF stimulation (Fig. S5 E), and these mRNAs were immediately transcribed after EGF treatment (Fig. 6 D). COL17A1 was also increased when keratinocytes were incubated with a matrix metalloproteinase (MMP) inhibitor, marimastat, but not with a neutrophil elastase inhibitor, sivelestat, or a serine protease inhibitor, aprotinin, even if the cells were not activated with EGF (Fig. 6 E). Among protease inhibitors that were up-regulated by EGFR activation, only TIMP1 has an inhibitory activity against MMPs (Murphy, 2011). Therefore, we assumed that TIMP1 is a target of EGFR signaling for the regulation of COL17A1 proteolysis.

TIMP1 (tissue inhibitor of metalloproteinases 1) is a natural inhibitor of MMPs and is released into the extracellular space. We confirmed that treatment with EGF increased the secretion of TIMP1 into the culture medium (Fig. 6 F) and increased the intracellular production of TIMP1 (Fig. 6 G). The addition of human recombinant TIMP1 to the culture increased COL17A1 expression, as did treatments with EGF or marimastat (Fig. 6 H). In contrast, COL17A1 was markedly decreased when keratinocytes were treated with an siRNA targeted for *TIMP1* (Fig. 6 I and S5 F). These results clearly indicate that EGFR signaling induces TIMP1 secretion and that TIMP1 inhibits COL17A1 proteolysis by suppressing metalloproteinase activity.

COL17A1 regulates human keratinocyte stem cell motility and maintenance

We next examined whether COL17A1 is associated with keratinocyte stem cell motility. Treatment with an siRNA targeting *COL17A1* efficiently suppressed COL17A1 expression in human keratinocyte cultures (Fig. S5, G and H). This *COL17A1* siRNA significantly decreased the rotational speed of two-cell colonies of keratinocytes (Fig. 7 A) and the cell locomotion speed of individual keratinocytes in the colonies (Fig. 7 B). The *COL17A1* siRNA also decreased the clonal growth of keratinocytes (Fig. 7 C) and increased the ratio of the stacking colony type in the culture (Fig. 7 D). COL17A1 was highly expressed in cells of expanding colonies (Fig. 7 E), and human keratinocytes treated with *COL17A1* siRNA had a decreased colony-forming efficiency after subcultivation (Fig. 7 F). These results indicate that COL17A1 promotes keratinocyte stem cell motility coupled with increased self-renewing capability.

COL17A1 is involved in reepithelialization by organizing actin and keratin filament networks

Collective cell migration drives reepithelialization (Rørth, 2009). We investigated whether COL17A1 is also involved in the collective migration of HaCaT human keratinocytes. HaCaT keratinocytes have a suppressed differentiation capacity under normal culture conditions, which can minimize the effects of differentiation-associated changes on cell behavior (Nanba et al., 2013b). We have previously established HaCaT cell lines expressing an emerald green fluorescent protein (EmGFP) and an shRNA construct targeting either *COL17A1* or scrambled (*SCR*; Liu

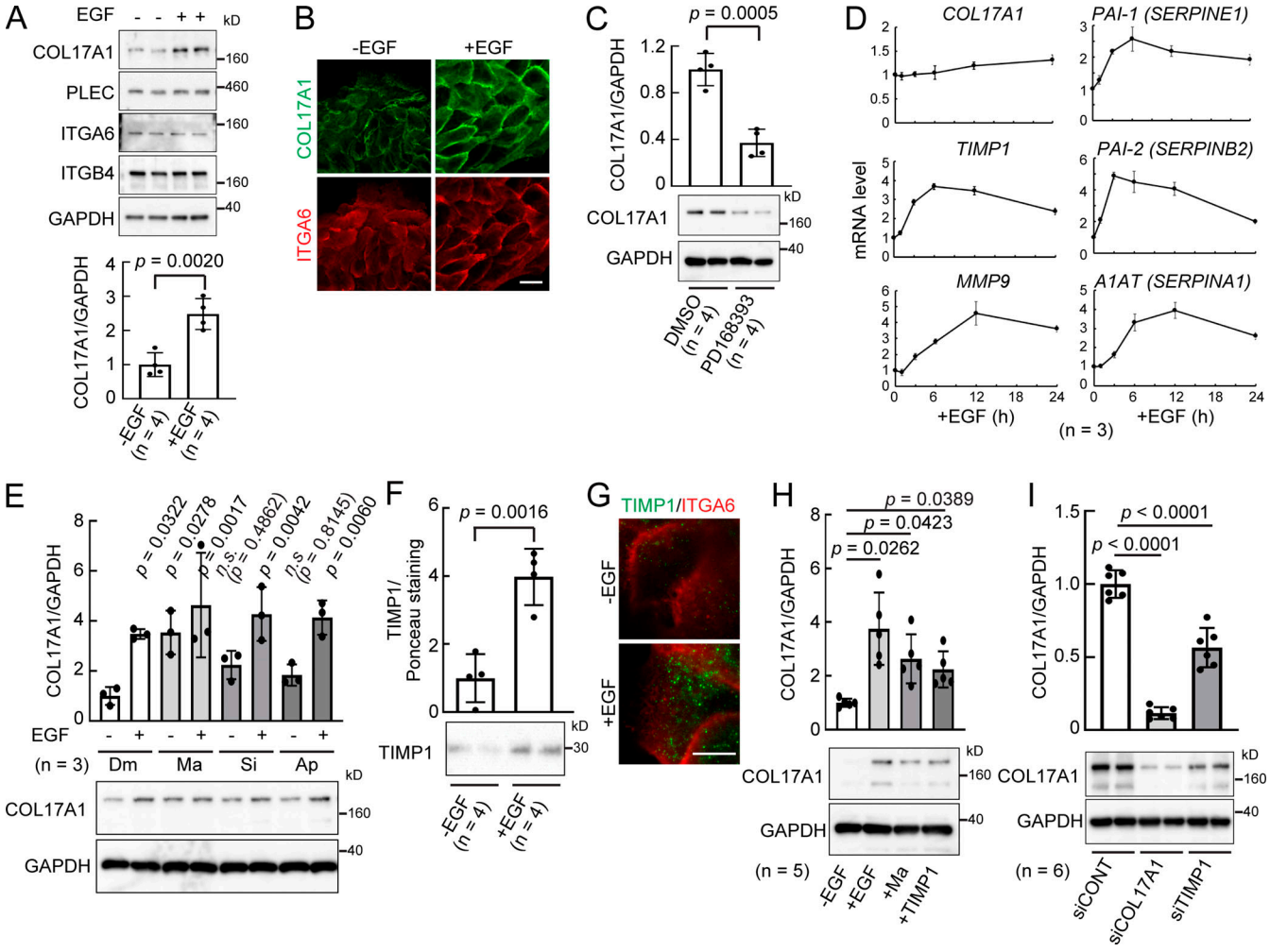

Figure 6. **EGFR signaling regulates COL17A1 proteolysis through TIMP1 secretion in keratinocytes. (A)** Expression of several hemidesmosomal proteins in human keratinocytes treated with and without EGF. **(B)** Immunostaining with anti-COL17A1 and anti-ITGA6 in keratinocytes treated with and without EGF. Scale bar, 20 µm. **(C)** Expression analysis of COL17A1 in keratinocytes treated with and without PD16839. **(D)** Time-course expression analysis of *COL17A1*, *TIMP1*, *MMP9*, *PAI-1*, *PAI-2*, and *A1AT* mRNAs by quantitative PCR. **(E)** Expression of COL17A1 in keratinocytes treated with protease inhibitors including marimastat (Ma), sivelestat (Si), or aprotinin (Ap) in the presence and absence of EGF. DMSO (Dm) was used as control. **(F)** Secretion of TIMP1 into the culture medium in response to EGF. TIMP1 secretion was normalized with the intensity of Ponceau staining of protein-transferred membranes. **(G)** Immunostaining with anti-COL17A1 and anti-TIMP1 in keratinocytes with and without EGF treatment. Scale bars, 10 µm. **(H)** Expression of COL17A1 in keratinocytes treated with EGF, Ma, or recombinant human TIMP1. **(I)** Expression of COL17A1 in keratinocytes treated with control, *COL17A1*-targeting, or *TIMP1*-targeting siRNA. P values were calculated with the two-tailed Student's *t* test in A, C, and F and one-way ANOVA with Dunnett's multiple comparisons test in E, H, and I.

et al., 2019). Reduced expression of COL17A1 by sh*COL17A1* was induced by treatment with doxycycline (Dox; Fig. S5 I), and the down-regulation of COL17A1 was confirmed by EmGFP expression (Fig. S5 J). Directed migration assays clearly revealed that sh*COL17A1*-expressing keratinocytes exhibit delayed closure of an epithelial gap (Fig. 8 A). While cell proliferation was also involved in the epithelial gap closure, directed cell migration and subsequent epithelial closure could be observed even though keratinocytes were diminished in most of their mitotic capacity by mitomycin C treatment (Figs. 8 B and S5 K). However, delayed collective migration elicited by knockdown of *COL17A1* was markedly enhanced, and incomplete closure of the epithelial gap could be observed with mitomycin C treatment (Fig. 8 B). This result indicated that COL17A1 was directly associated with keratinocyte motility.

Interactions of actin and keratin filaments are required for well-organized collective cell migration (van Bodegraven and Etienne-Manneville, 2020). In HaCaT keratinocytes localized at the leading edge of expanding HaCaT colonies, actin microfilaments were localized at the periphery of cells, and keratin intermediate filaments were placed inside the peripheral actin filament networks (Fig. 8 C). However, knockdown of *COL17A1* decreased the area of peripheral actin networks, and keratin filaments extended into the periphery of cells (Fig. 8, D and E). COL17A1 is connected to the keratin intermediate filaments via the intracellular scaffold protein plectin (PLEC) that is also associated with actin microfilaments (Tsuruta et al., 2011). PLEC was colocalized with COL17A1 at the periphery of HaCaT keratinocytes (Fig. 8 F). Intriguingly, PLEC was delocalized in sh*COL17A1*-expressing keratinocytes (Fig. 8 G). These results

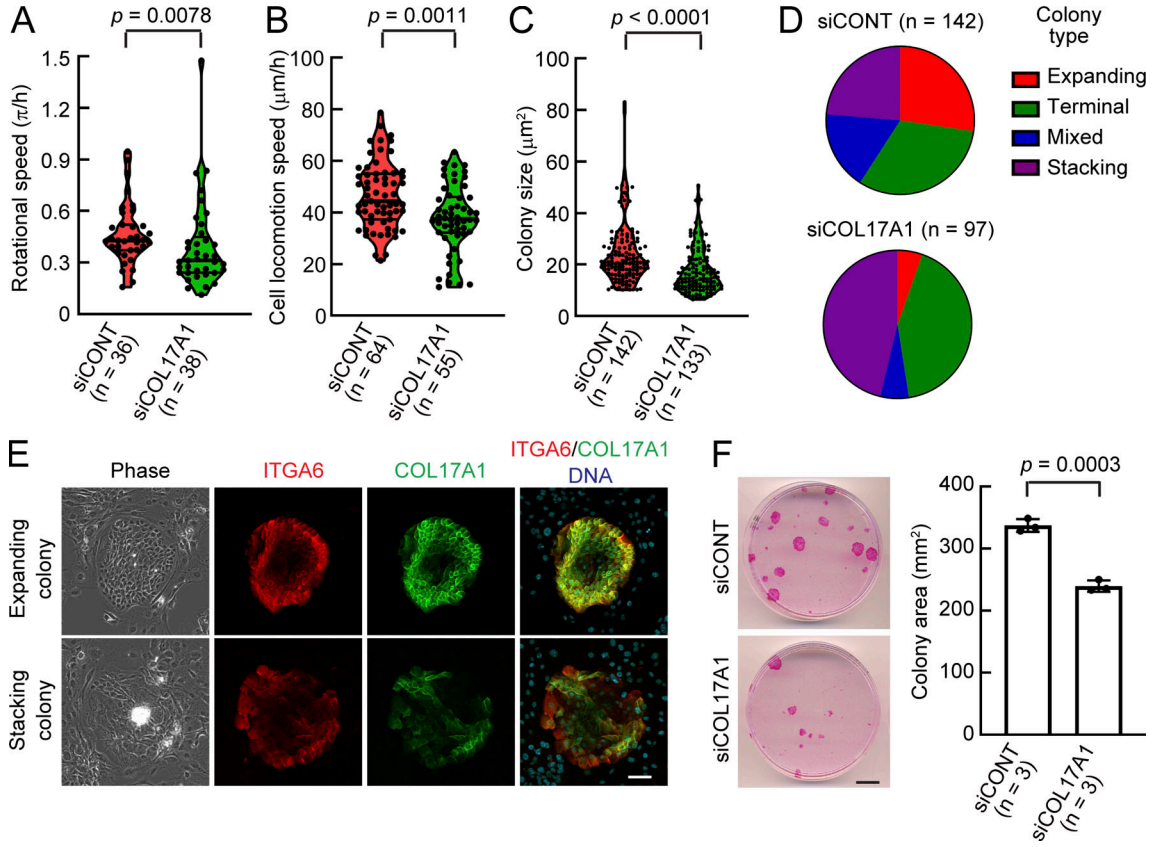

Figure 7. **COL17A1 is involved in keratinocyte stem cell motility and maintenance. (A)** Distribution of rotational speed of two-cell colonies of human keratinocytes treated with control siRNA or *COL17A1*-targeting siRNA on culture day 1. **(B)** Distribution of locomotion speed of individual cells in human keratinocyte colonies treated with a control siRNA or a *COL17A1*-targeting siRNA on culture day 2. **(C)** Distribution of colony size in keratinocyte cultures treated with control siRNA or *COL17A1*-targeting siRNA on culture day 4. **(D)** Distribution of colony types in keratinocyte culture treated with control siRNA or *COL17A1*-targeting siRNA on culture day 6. **(E)** Expression of COL17A1 and ITGA6 in expanding and stacking colonies. Scale bar, 100 µm. **(F)** Colony-forming efficiency of human keratinocytes treated with a control siRNA or with a *COL17A1*-targeting siRNA. The values reported (mean ± SD) were obtained from the total colony area in each culture dish. Scale bar, 10 mm. P values were calculated with the two-tailed Mann–Whitney *U* test in A–C and the two-tailed Student's *t* test in F.

indicate that COL17A1 regulates actin and keratin filaments with PLEC and coordinates cell motility to enhance cell migration (shown schematically in Fig. 9).

Discussion

The alteration of keratinocyte stem cell dynamics is assumed to be involved in the age-dependent decline of skin regenerative capacity, but the underlying mechanism is unknown. Cell locomotion in human keratinocyte colonies was first reported >40 yr ago by Sun and Green (1976), and recent studies have revealed that cell motility is associated with the proliferative capacity of human epidermal and oral keratinocytes (Hirose et al., 2021; Hoshikawa et al., 2021; Hoshikawa et al., 2019; Kinoshita et al., 2019; Nanba et al., 2015; Tate et al., 2015). Here we demonstrated that an age-dependent decline of EGFR signaling impairs keratinocyte stem cell motility and reepithelialization through COL17A1 proteolysis.

Age-associated impaired wound healing arises from intrinsic and extrinsic defects of keratinocyte migration (Keyes et al., 2016). Our wound healing experiments revealed the age-associated decline of EGFR phosphorylation in mouse skin wounds, which can be explained by the local or systemic reduction of EGFR ligands. Indeed, age-related decreases of EGF in urinary excretion (Uchihashi et al., 1982), serum (Shurin et al., 2007), and burn injury (Farinas et al., 2018) in humans have been reported. Several randomized controlled clinical trials have concluded that topical application and intralesional injection of human recombinant EGF promote the healing of diabetic foot ulcers (Yang et al., 2020), suggesting that the age-associated decline of EGFR signaling due to the decreased production of EGFR ligands is involved in ulcer formation and/or impaired wound healing.

We revealed that EGFR activation suppresses COL17A1 proteolysis through the secretion of TIMP1. COL17A1 regulates keratinocyte stem cell motility by coordinating actin microfilaments and keratin intermediate filaments. Several studies have demonstrated that COL17A1 is involved in keratinocyte motility, but the results are controversial. Some studies have reported that COL17A1 deficiency enhances the spontaneous migration of single keratinocytes (Jacków et al., 2016a; Löffek et al., 2014) and directed migration of keratinocytes in a scratch wound assay (Tasanen

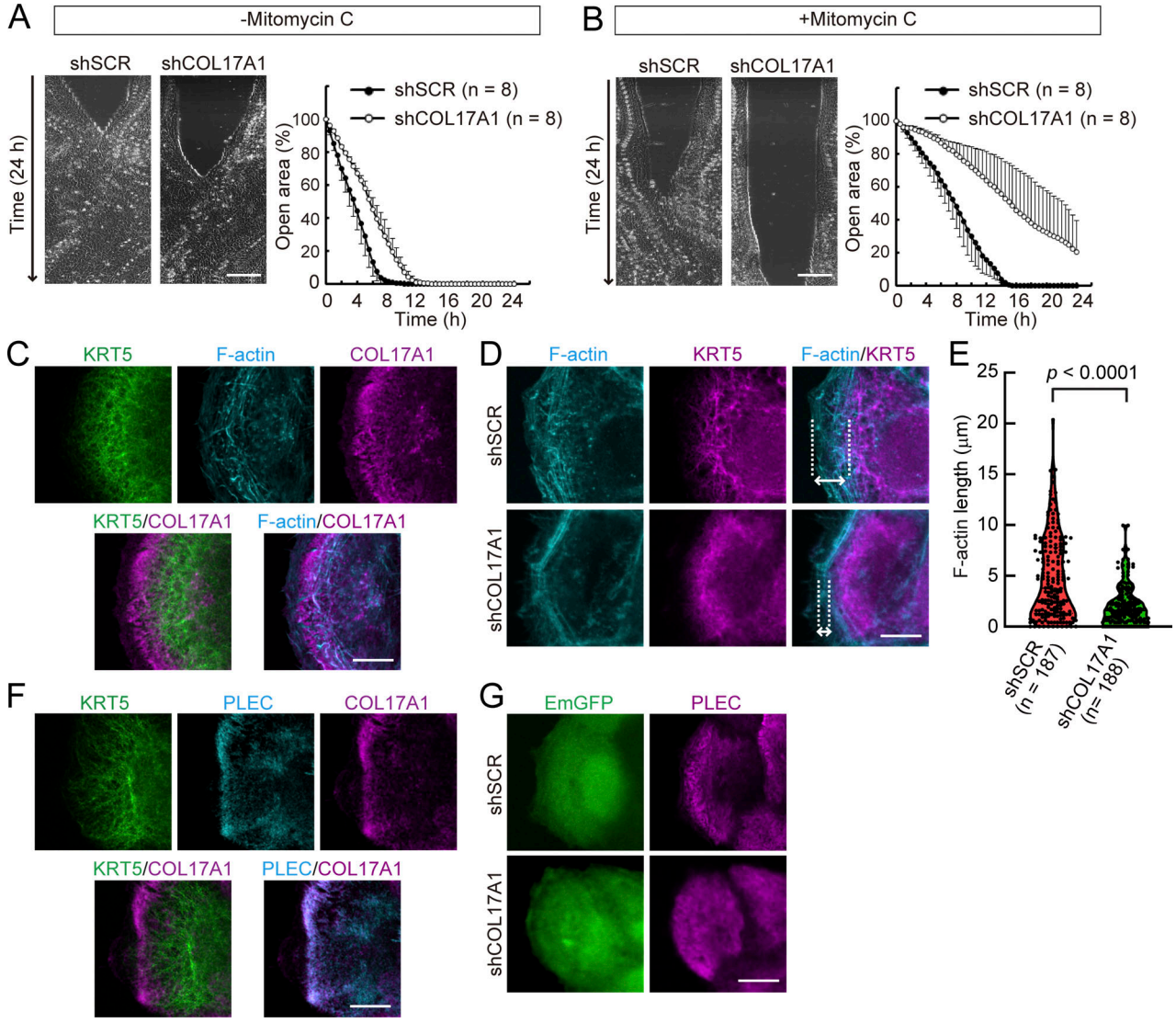

Figure 8. **COL17A1 regulates keratinocyte motility by coordinating cytoskeletal networks. (A and B)** Directed migration assay using SCR or *COL17A1*-targeting shRNA expressing HaCaT keratinocytes in −mitomycin C (A) and +mitomycin C (B) conditions. Left: Representative kymographs of directed cell migration. Right: Quantification (mean ± SD) of uncovered areas. Scale bars, 200 µm. **(C)** Representative immunofluorescence images of HaCaT cells with anti-KRT5 and anti-COL17A1. F-actin was also visualized with Alexa Fluor 647–conjugated phalloidin. Scale bar, 10 µm. **(D)** Distribution of F-actin and KRT5 in HaCaT cells expressing SCR or *COL17A1*-targeting shRNA. Two-dotted lines indicate F-actin–rich and KRT5-absent region. Scale bar, 10 µm. **(E)** Distribution of the length of F-actin–rich and KRT5-absent regions in HaCaT cells expressing SCR shRNA or *COL17A1*-targeting shRNA. **(F)** Representative immunofluorescence images of HaCaT cells with anti-KRT5, anti-PLEC, and anti-COL17A1. Scale bar, 10 µm. **(G)** Distribution of PLEC in HaCaT cells expressing SCR shRNA or *COL17A1*-targeting shRNA. shRNA expression was confirmed with GFP expression. Scale bar, 10 µm. P value was calculated with the two-tailed Mann–Whitney *U* test in E.

et al., 2004). However, other studies have shown that COL17A1 knockdown impairs directed migration of single keratinocytes (Hamill et al., 2011; Hiroyasu et al., 2016). We have demonstrated here that the reduced expression of COL17A1 decreases the spontaneous migration of keratinocytes in the colony and the directed collective migration of keratinocytes. Previously, we also demonstrated that skin wound healing in mice is suppressed by COL17A1 deficiency and is accelerated by forced expression of COL17A1 (Liu et al., 2019). Furthermore, mice expressing uncleavable COL17A1 also exhibited an enhanced reepithelialization phenotype (Jacków et al., 2016b). Collectively, these results indicate that COL17A1 is essential for the collective migration of keratinocytes and for reepithelialization by enhancing keratinocyte stem cell motility.

Altered organization of actin microfilaments by a deficiency of COL17A1 has been reported (Jacków et al., 2016a; Löffek et al., 2014). In this study, we demonstrated that decreased expression of COL17A1 causes disorganized remodeling of actin and keratin filaments and disturbs distribution of PLEC. PLEC mediates the linkage of keratin filaments to COL17A1 and α6β4 integrin that directly bind to extracellular laminin-332 and is involved in both actin and keratin dynamics (Moch et al., 2016; Tsuruta et al., 2011; van Bodegraven and Etienne-Manneville, 2020). While it remains unknown how the reduced expression of COL17A1

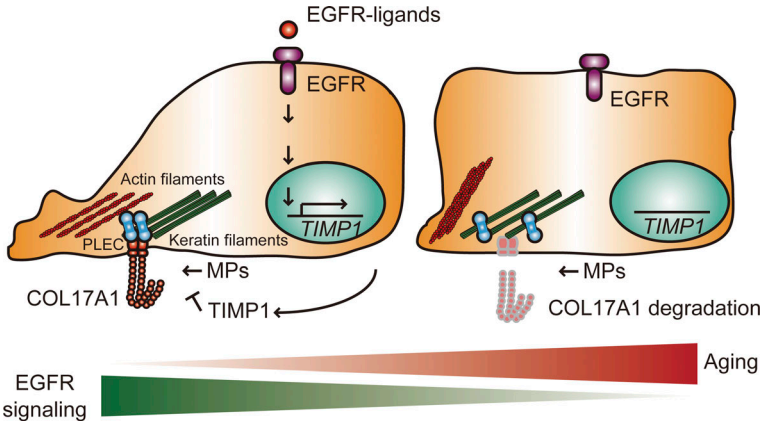

Figure 9. **Schematic drawing of EGFR-mediated keratinocyte stem cell motility regulated by COL17A1 proteolysis.** EGFR signaling stabilizes COL17A1 through TIMP1 induction, which is required for cell motility coordinated by actin and keratin filament networks. The age-associated decline of EGFR signaling results in impaired reepithelialization and skin regeneration. MPs, metalloproteinases.

affects PLEC distribution and cytoskeletal filaments, it has been reported that disrupted interaction between PLEC and COL17A1 results in epidermolysis bullosa simplex (Natsuga et al., 2017). Furthermore, COL17A1 knockdown impairs the interaction between BPAG1 (Dystoin) and α6β4 integrin (Hamill et al., 2011). These results strongly suggest that reduction of COL17A1 results in hemidesmosome disassembly and decreases the cell-basement membrane interaction, which is required for horizontal keratinocyte migration and epidermal integrity. Skin reepithelialization is often delayed in hemidesmosome instability diseases (Peking et al., 2018), possibly due to disorganized actin and keratin filaments at the leading edge of migrating keratinocytes, as seen in this study. Although further investigations are still required, COL17A1 stabilization by regulating its proteolysis is a candidate therapeutic approach for the improvement of age-associated impaired skin regeneration, including ulcers.

Materials and methods

Preparation of feeder cells

3T3-J2 cells were cultivated at 37°C and 10% CO_2 in DMEM (Gibco BRL; 11995-065) supplemented with 10% bovine serum (Sigma-Aldrich; C8056). The 3T3-J2 cells were passaged once a week and maintained up to passage 12 with medium changes every 3 or 4 d. To prepare the feeder layer, 3T3-J2 cells were incubated with 4 µg/ml mitomycin C (Kyowa Kirin) for 2 h and washed twice with PBS. The mitomycin C–treated 3T3-J2 cells were then trypsinized and seeded as feeder cells before the inoculation of keratinocytes.

Human keratinocyte cultures

Normal human epidermal keratinocytes were isolated from neonatal, infant, and adult human skin. Isolated keratinocytes were expanded ex vivo and preserved in a liquid nitrogen container. Frozen keratinocytes were thawed and cultivated at clonal density on a feeder layer of mitomycin C–treated 3T3-J2 cells, at 37°C and 10% CO_2 in FAD medium (a 3:1 mixture of DMEM and Ham's F12 medium [Gibco BRL; 11765-054]) and 1.8 × 10^{-4} M adenine hemisulfate salt (Sigma-Aldrich; A3159)) supplemented with 10% FBS (Biowest; 91760-500), 5 µg/ml insulin (Sigma-Aldrich;; I5500), 0.4 µg/ml hydrocortisone (Calbiochem; 386698), 10^{-10} M cholera toxin (MP Medicals; 190329), and 2 × 10^{-9} M triiodothyronine (Sigma-Aldrich; T2752), as described previously (Rheinwald and Green, 1975; Rochat et al., 1994). Keratinocytes were used between passages 2 and 7. The medium was changed after 4 d of cultivation to medium containing 10 ng/ml recombinant human EGF (Upstate Biotechnology; 01-107). The medium was changed every 4 d. Keratinocytes were also treated with 10 µM PD168393 (Calbiochem; 513033), 1.5 µg/ml recombinant human TIMP1 (PeproTech; 410-01), 3 µM marimastat (Sigma-Aldrich; M2699), 3 µM sivelestat (Enzo; BML-PI157), and 3 µM aprotinin (Takara; T010A), depending on the experimental conditions. This study was approved by the ethics committees of the Medical Research Institute, Tokyo Medical and Dental University (2015-6), and the Ehime University School of Medicine (1810004 and 1904015).

Clonal analysis was performed as described previously (Barrandon and Green, 1987b). In brief, human keratinocytes were cultivated at clonal density on a feeder layer of mitomycin C–treated 3T3-J2 cells, and isolated colonies were individually trypsinized in a cloning ring and subcultured into a 60-mm cell culture dish. To visualize keratinocyte colonies, cultures were fixed with 3.7% buffered formaldehyde and stained with 1% rhodamine B (Sigma-Aldrich; R6626).

For EGF stimulation experiments, keratinocytes were grown in complete growth medium for 7 d and further incubated in basal medium for 24 h before EGF stimulation. Keratinocytes were harvested after 48-h incubation with and without EGF and analyzed by Western blotting and quantitative PCR.

Explant cell cultures using human skin samples

The subject was a patient with CLI and diabetic nephropathy undergoing hemodialysis. The foot wound was initially treated with percutaneous transluminal angioplasty to increase lower limb blood flow for limb salvage, and subsequently with minor amputation. Redundant healthy skin adjacent to the foot wounds, which occurred after surgical stump closure, was examined. As autologous skin grafts after minor amputation were required, redundant donor skin taken from the trunk for skin grafting was used as the control. This study was approved by the Ethics Committees of the International University of Health and Welfare (5-16-12), Medical Research Institute, Tokyo Medical and Dental University (02016-008 and 02018-005), and Takatsu General Hospital (CR-1607 and CR-18-08). Explant cell cultures using human skin fragments were performed as reported

previously (Toki et al., 2020). Briefly, the skin was cut into small pieces and then plated on 60-mm cell culture dishes with human keratinocyte culture medium. The skin fragments were then incubated for 2–3 wk at 37°C and 10% CO_2. Seven keratinocyte migrations from human skin fragments isolated from an unaffected region (trunk) of a patient with CLI and eight keratinocyte migrations from the human skin fragments isolated from an affected region of the patient were analyzed.

Immunofluorescence microscopy

Keratinocytes were seeded at clonal density in 35-mm cell culture dishes (Grainer Bio-one; 627965) with mitomycin C–treated 3T3-J2 cells and grown for 7 d at 37°C and 10% CO_2. The cells were fixed in 4% PFA in PBS for 20 min and treated with 0.1% Triton X-100 in PBS for 10 min at RT. After treatment with 1% BSA, the cells were incubated with primary antibodies overnight at 4°C, washed in PBS, and incubated with appropriate secondary antibodies for 1 h at RT. The cells were also treated with Hoechst 33342 (Molecular Probes; H1399) and Alexa Fluor 488–, Alexa Fluor 647–, or rhodamine-conjugated phalloidin (Molecular Probes; A12379, A22287, and R415) to visualize nuclei and actin filaments, respectively. After a wash with PBS, cells were mounted with PermaFluor mounting medium (Thermo Fisher Scientific; TA-030-FM) and examined using an FV10i confocal microscope (Olympus) with 10×/0.4 and 60×/1.2 lenses (Olympus). Image acquisition was performed with Fluoview software (Olympus).

Primary antibodies used for immunofluorescence microscopy were as follows: rat monoclonal antibody against ITGA6 (BD PharMingen; 555734, 1:200), mouse monoclonal antibody against α-tubulin (Sigma-Aldrich; T6199, 1:500), mouse monoclonal antibody against KRT10 (Santa Cruz Biotechnology; SC-52318, 1:50), rabbit polyclonal antibody against loricrin (BioLegend; 905101, 1:100), mouse monoclonal antibody against IVL (Abcam; ab68, 1:500), rabbit monoclonal antibody against COL17A1 (Abcam; ab186415 and ab184996, 1:200), mouse monoclonal antibody against TIMP1 (Thermo Fisher Scientific; MS-608, 1:100), rabbit polyclonal antibody against KRT5 (Abcam; ab53121, 1:500), chicken polyclonal antibody against KRT5 (BioLegend; 905904, 1:200), and guinea pig polyclonal antibody against PLEC (PROGEN; gp21, 1:500). Secondary antibodies used for immunofluorescence microscopy were as follows: Alexa Fluor 488–conjugated donkey antibody against mouse IgG (Molecular Probes; A21202, 1:200), Alexa Fluor 488–conjugated donkey antibody against rat IgG (Molecular Probes; A21208, 1:200), Alexa Fluor 594–conjugated donkey antibody against rat IgG (Molecular Probes; A21209, 1:200), Alexa Fluor 488–conjugated donkey antibody against rabbit IgG (Molecular Probes); Alexa Fluor 594–conjugated donkey antibody against rabbit IgG (Molecular Probes; A21207, 1:200), Alexa Fluor 647–conjugated donkey antibody against rabbit IgG (Molecular Probes; A32795, 1:200), Alexa Fluor 488–conjugated donkey antibody against chicken IgY (Jackson ImmunoResearch Laboratories; 703-545-155, 1:200), and Alexa Fluor 594–conjugated goat antibody against guinea pig IgG (Jackson ImmunoResearch Laboratories; 706-586-148, 1:200).

Time-lapse imaging, lineage, and cell behavior analysis

Human epidermal keratinocytes were seeded at clonal density in 35-mm cell culture dishes (Grainer Bio-one; 627965) on a feeder layer of mitomycin C–treated 3T3-J2 cells and grown at 37°C and 10% CO_2. For time-lapse imaging, cells were maintained at 37°C and 5% CO_2 in a chamber mounted on a microscope (FV10i; Olympus) with 10×/0.4 lens (Olympus). Image acquisition was performed with Fluoview software (Olympus). Images were obtained at 5-min intervals for 1–96 h, depending on the experimental conditions. Lineage trees were described by manual analysis of serial images obtained from time-lapse experiments. Six expanding and nine stacking colony formations were analyzed.

Three patterns of cell fate determination after cell division were defined according to the classification by Roshan et al. (2016). We categorized cultured keratinocytes into two types: proliferative (P) or differentiating (D) cells, which divided or did not divide within 48 h, respectively. Keratinocytes that could not be tracked for 48 h were excluded from further analysis. PP divisions were defined in cases where one P cell symmetrically divides and produces two proliferative cells. DD divisions were defined in cases where one P cell symmetrically divides and produces two D cells. Asymmetric PD divisions were defined in cases where one P cell divides and produces one P and one D cell.

Two modes of keratinocyte behavior after cell division were defined as follows. The expanding mode was defined in cases where two daughter cells produced by planar cell division remained in the basal layer. The expanding mode was defined in cases where one or two daughter cells produced by planar cell division in the basal layer moved toward the suprabasal layer and remained there for at least several hours. It was sometimes observed that one or two daughter cells in the suprabasal layer generated by the stacking mode of behavior migrated down to the basal layer and proliferated there within 48 h. Therefore, the two modes of cell behavior after cell division can occur but are associated with three types of cell fate determination. The frequency of the two modes of cell behavior was calculated from 24-h observations of the formation of each type of colony on culture days 2 and 3, respectively.

Measurement of cell cycle duration, cell locomotion, and rotational speed

Time-lapse images were acquired with an FV10i microscope (Olympus) and Fluoview software (Olympus) and analyzed with Fiji (Schindelin et al., 2012). Cell cycle duration was defined as the duration between two rounds of cell division. Cell locomotion speed was defined as the amount of change in the position of the cell nucleus. The position of the nucleus in the cell was given as the center of the circle that approximated the nuclear shape. The rotational speed of a two-cell colony was assessed as the amount of change in the angle between cells in a two-cell colony. The angle of contact surface between cells in a two-cell colony was given by the top-right angle of the contact surface against the perpendicular axis.

Lentiviral production and infection

A plasmid for lentiviral expression of NLS-EGFP.P2A.CAAX-mCherry was generated by subcloning the NLS-EGFP.P2A.CAAX-mCherry cDNA from pcDNA3.1-Hyg-NLS-EGFP.P2A.Cherry.CAAX into the HIV-based self-inactivating lentiviral

expression vector plasmid pCSII-CMV-MCS (RIKEN BioResource Center). For lentiviral production, 293FT cells were transfected with the expression plasmid and packaging plasmid DNAs (pCAG-HIVgp and pCMV-VSV-G-RSV-Rev; RIKEN BioResource Center) using Lipofectamine 2000 (Invitrogen; 11668019). Keratinocytes were then infected by replacing the infection medium containing lentiviral particles and polybrene (hexadiamine bromide; Sigma-Aldrich; H9268) as previously described (Nanba et al., 2013a). pcDNA3.1-Hyg-NLS.EGFP.P2A.Cherry.CAAX was a gift from Dr. Bertrand Collet (Université Paris-Saclay, Paris, France; Addgene plasmid 52421; RRID:Addgene_52421).

Measurement of cell division axis

The angle of the cell division axis in a dividing keratinocyte was defined as an acute crossed-axes angle ($0 \le \theta \le \pi/2$) between a line linking two centrosomes and the basal plane (see also Fig. S2 B). The angles of the cell division axis were measured with Fiji (Schindelin et al., 2012).

Cell kinetic modeling and computer simulation

We defined a cell with a round shape with a radius r = 10 µm on average with an extension of d = 2 µm. When there is one cell, it does not move and remains calmly at a position. After cell division, two cells stick to each other by touching softly at a distance of approximately $|\mathrm{r}(\rightarrow)_1 - \mathrm{r}(\rightarrow)_2| = 2 \times (r + d) = 24$ µm, where the positions of the two cells are written as $\mathrm{r}(\rightarrow)_1$ and $\mathrm{r}(\rightarrow)_2$. These two cells stick to the basal surface and, at the same time, rotate around each other. We included cell growth so that the volume of a cell doubles during the cell division cycle. The standard division cycle was 14 h, and the average cell had a radius r = 10 µm. We allowed that the division cycle had a constant distribution between 12 and 16 h. This division cycle was assigned randomly for each cell when it was born, and the divided cells have half the volume of the parent cell. The natural growth of cells pushes other cells when many cells touch each other and brings them to an equilibrium distance of $r_e = r_1 + r_2 + 2d$ by pushing against each other.

We defined the rotational motion of a target cell as the rotation of other cells around the target cell. A cell rotates around the other cell while keeping the distance between the two cells unchanged. In the simulation, we set the time step as a minute. Below the equilibrium distance, the cells rotate with the same angular velocity. Above the equilibrium distance, the rotational speed (ω) decreases with the distance: $\omega\,(r_{12}) = \omega_0 \exp\,[-(r_{12} - r_e)/d]$, where r_{12} is the distance between two cells. As cell development proceeds, the motion of cells toward the middle of a colony becomes slow because the motion is hindered by other surrounding cells. Hence, we introduced a process to reverse the rotational axis when the cell number in the basal layer becomes more than n_0 = 50. In this case, the rotational motion of two cells with opposite rotational axis becomes a translational motion so that some space can be made in the middle part of a colony. We arranged the computer simulation so that the number of oppositely rotating cells becomes ∼50% of the total number.

For the cell division, there should be enough space for two cells to be born from one large cell at the time of cell division. We defined that the divided cells also have round shapes. The two daughter cells do not fit in the space the parent cell has occupied. In case there are no other cells surrounding the parent cell, the two daughter cells can be placed at the basal layer. However, if the parent cell is surrounded by other cells, the daughter cells move up to the second layer (suprabasal layer 1) above other surrounding cells in the basal layer. In this case, there might be other cells already present in that space. When there is this conflict in the suprabasal layer 1, the preexisting cells in the suprabasal layer 1 are pushed up to the third layer (suprabasal layer 2). The cells staying in the suprabasal layers can move down to lower layers when there are no other cells under them. The cells in the suprabasal layers can also move down to lower layers when other cells are outside their size.

We introduced a boundary circle for colony growth, whose radius was R_b. The radius of the boundary of a colony is defined as $R_b = (4/\pi \cdot r^2 \cdot n)^{1/2} + C$. Cells can move freely within this circle, but due to the rotational motion of cells, some cells may hit the boundary. In this case, the cells are pushed back within the circle without losing their velocities. We formulated this situation by assigning a new position as $|\mathrm{r}(\rightarrow)_{new}| = 2R_b - |\mathrm{r}(\rightarrow)_{sim}|$, where $\mathrm{r}(\rightarrow)_{sim}$ is the position of a cell calculated by the above procedures and the new position is $|\mathrm{r}(\rightarrow)_{new}|$ when the cell is outside the circle.

After all the above preparations, we ran a simulation of colony growth from one stem cell. We included the rotational motion, natural cell growth, cell division, move-up and move-down processes, and all the necessary adjustment of cells in a colony. We took the simulation time step as a minute. With this setup, we created a Fortran program to simulate the movement of cells in a colony with various rotational speeds. We used a random number generator to confer these parameters to the cells, and five independent calculations with different random seeds were performed. The Fortran program is provided in Data S1.

Wound healing experiments

C57BL/6N mice were purchased from the Sankyo Laboratory Service. 12-week-old (n = 3) and 19–25-mo-old (n = 3) male mice were used as young and old mice in the experiments, respectively. Before wounding, mice were anesthetized using isoflurane (Pfizer), and the absence of a physical and physiological response to a noxious stimulus was verified. A punch biopsy was performed using a 6-mm-diameter biopsy punch (Kai Industries; BP-60F) to make a circular full-thickness wound on the dorsal skin. 3 d after wounding, all mice were euthanized, and the wounded area was excised from the skin. An ∼2-mm margin of the wound was collected for further experiments. Mouse care was in accordance with the guidance of the Tokyo Medical and Dental University for mouse experiments. All mouse experiments were performed according to the Guidelines for the Care and Use of Laboratory Animals and were approved by the Institutional Committee of Laboratory Animals.

Phospho-RTK array

Phosphorylated RTKs were detected using a mouse phospho-RTK array kit (R&D Systems; ARY014), according to the manufacturer's instructions.

EdU experiments

To label cells with active DNA synthesis, the thymidine analogue EdU was added to the cultures at 10-μM concentration 24 h before fixation. After the removal of feeder cells by gentle pipetting, the cells were fixed in 4% PFA in PBS for 20 min and treated with 0.5% Triton X-100 in PBS for 20 min at RT. Incorporated Edu was detected using a Click-iT Plus Alexa Fluor 488 EdU Imaging Kit (Molecular Probes; C10637). After treatment with 1% BSA, the cells were incubated with rat monoclonal antibody against ITGA6 overnight at 4°C, washed in PBS, and incubated with Alexa Fluor 488–conjugated donkey antibody against rat IgG for 1 h at RT. The cells were also treated with Hoechst 33342 to visualize nuclei. After washing with PBS, cells were examined using an FV10i confocal microscope (Olympus). Image acquisition was performed with Fluoview software (Olympus).

Western blotting

After the removal of 3T3 feeder cells by gentle pipetting, keratinocytes were lysed with cell lysis buffer (150 mM NaCl, 10 mM Tris-HCl, 1 mM EDTA, and 1% NP-40) containing a protease inhibitor cocktail (Roche; 04 693 159 001) and a phosphatase inhibitor cocktail (Roche; 04 906 837 001). The skin fragments were also homogenized and lysed in the same lysis buffer. Conditioned medium from keratinocyte cultures was concentrated by acetone precipitation. After measurement of the protein concentration of each lysate using a BCA Protein Assay Kit (Pierce; 23227), equal amounts of proteins were solubilized in SDS sample buffer and separated by SDS-PAGE. Proteins in the gels were then transferred to PVDF membranes (Millipore; IPVH304F0). After blocking with Blocking One (Nacalai Tesque; 03953-95), the membranes were immunoblotted with primary antibodies diluted in Blocking One overnight at 4°C. After washing with 1× TBST (25 mM Tris-HCl, pH 7.4, 150 mM NaCl, and 0.1% Tween-20), the membranes were incubated with HRP-conjugated secondary antibodies against mouse IgG (Amersham; NA931, 1:5,000) or rabbit IgG (Amersham; NA934, 1:5,000) for 1 h at RT. After washing with TBST, the membranes were treated with Immobilon Forte Western HRP Substrate (Millipore; WBLUF0100), and chemiluminescence signals were detected with FUSION Solo S (Vilber Lourmat). Protein loading and transfer was confirmed with Ponceau-S staining solution (Beacle; BCL-PSS-01). Primary antibodies used for Western blotting were as follows: rabbit monoclonal antibody against EGFR (Abcam; ab52894, 1:1,000), rabbit polyclonal antibody against phospho-EGFR (Tyr845; Millipore; 07-820, 1:1,000), rabbit polyclonal antibody against ErbB2 (Cell Signaling Technology; 2165, 1:1,000), rabbit polyclonal antibody against phospho-ErbB2 (Tyr1248; Cell Signaling Technology; 2247, 1:1,000), mouse monoclonal antibody against COL17A1 (Covance; SIG-3780, 1:500), mouse monoclonal antibody against PLEC (Cosmo Bio; NU-01-PLC, 1:200), rabbit polyclonal antibody against ITGA6 (Abcam; ab97760, 1:1,000), rabbit polyclonal antibody against ITGB4 (Santa Cruz Biotechnology; sc-9090, 1:1,000), rabbit monoclonal antibody against ITGB1 (Abcam; ab179471, 1:1,000), rabbit polyclonal antibody against GAPDH (Cell Signaling Technology; 2118, 1:5,000), and mouse monoclonal antibody against TIMP1 (Thermo Fisher Scientific; MS-608, 1:250). Chemiluminescence signals were quantified using Fiji (Schindelin et al., 2012). GAPDH expression was used as a loading control. Western blotting images are representative of at least three independent experiments, and the values reported (mean ± SD) were obtained from at least three independent loadings in each figure.

Quantitative RT-PCR

Total RNAs were extracted from cultured keratinocytes using a GenElute mammalian total RNA miniprep kit (Sigma-Aldrich; RTN70). cDNAs were synthesized from 2 μg of total RNA using a High Capacity cDNA Reverse Transcription kit (Applied Biosystems; 4368813), according to the manufacturers' instructions. Quantitative PCR was performed using a SYBR Green qPCR Kit (Agilent Technology) and a Mx3000P Real-Time QPCR System (Agilent Technology). Relative levels of expression were determined by normalization to *GAPDH* using the ΔΔCt method. The values reported (mean ± SD) were obtained from triplicate experiments. The primer sequences used were as follows: human *COL17A1*, 5′-AGCGGCTACATAAACTCAACTGG-3′, 5′-CCGTCC TCTGGTTGAAGAAG-3′; human *ADAM9*, 5′-TGTGGGAACAGT GTGTTCAAGGA-3′, 5′-CCAATTCATGAGCAACAATGGAAG-3′; human *ADAM10*, 5′-CTGCCCAGCATCTGACCCTAA-3′, 5′-TTG CCATCAGAACTGGCACAC-3′; human *ADAM17*, 5′-CACCTGAAG AGCTTGTTCATCG-3′, 5′-TACTCTCTTCCCCTCTGCCC-3′; human *MMP9*, 5′-CGGTTTGGAAACGCAGATGG-3′, 5′-TGGGTG TAGAGTCTCTCGCT-3′; human *ELANE*, 5′-AACGACATCGTG ATTCTCCAG-3′, 5′-GATTAGCCCGTTGCAGACCAA-3′; human *SERPINE1*, 5′-GGGCCATGGAACAAGGATGA-3′, 5′-CTCCTTTCC CAAGCAAGTTG-3′; human *SERPINB1*, 5′-GTACTTGCGTGAAAA GC-3′, 5′-TCTCCGACATCCCTGA-3′; human *SERPINA1*, 5′-GTC AAGGACACCGAGGAAGA-3′, 5′-TATTTCATCAGCAGCACCCA-3′; human *TIMP1*, 5′-TTCTGGCATCCTGTTGTTGCTG-3′, 5′-GGT GGTCTGGTTGACTTCTGGTGT-3′; human *TIMP2*, 5′-TGGGAC ACCCTGAGCACCAC-3′, 5′-GTTGATGTTCTTCTCTGTGACCCA GTC-3′; human *TIMP3*, 5′-GAACTATCGGTATCACCTGGGTTG TAAC-3′, 5′-GATGCAGGCGTAGTGTTTGGACT-3′; and human *GAPDH*, 5′-ACCACAGTCCATGCCATCAC-3′, 5′-TCCACCACCCTG TTGCTGTA-3′.

Transfection of siRNAs into normal human epidermal keratinocytes

siRNAs were transfected into human keratinocytes using Lipofectamine RNAiMAX reagent (Invitrogen) according to modified manufacturer's instructions. Briefly, the prepared RNAiMAX liposome solution containing 2 μl of RNAiMAX and 2 μl of 10 μM siRNA in 500 μl Opti-MEM solution (Gibco) was immediately added into a well of a 6-well plate or a 35-mm dish after inoculation. The cells were then analyzed ≥24 h after the transfection. siRNAs used in this study were as follows: control siRNA-B (Santa Cruz Biotechnology; sc-44230), COL17A1 siRNA (human; Santa Cruz Biotechnology; sc-43070), TIMP1 siRNA (human; Santa Cruz Biotechnology; sc-29505), and MISSION siRNA universal negative control #1 (Sigma-Aldrich; SIC-001).

Directed migration assay

HaCaT keratinocytes stably expressing shRNA targeting human COL17A1 and SCR were previously established (Liu et al., 2019)

and were maintained in DMEM with 10% FBS. For the directed migration assay, these HaCaT cell lines were prepared at 0.8 × 10^6 cells/ml in DMEM with 10% FBS containing 500 ng/ml Dox (Wako; 04931121), and a 70-µl volume of the suspension was seeded into each well of a Culture-Insert 2 well (Ibidi; 81176) on a 35-mm cell culture dish (Grainer Bio-one; 627965) and incubated overnight. After treatment with and without 0.4 µg/ml mitomycin C (Kyowa Kirin) for 2 h and further incubation with DMEM with 10% FBS containing 500 ng/ml Dox, the culture insert was removed from the cell culture dish, and serial images were obtained at 30-min intervals for 24 h. Time-lapse images were acquired with an FV10i microscope (Olympus) and Fluoview software (Olympus).

Statistical analysis

Prism8 software (GraphPad) was used to assess statistical significance. To determine significance between two groups, comparisons were performed using an unpaired two-tailed Student's *t* test or Mann–Whitney *U* test. For multiple comparisons, one-way ANOVA with Dunnett's post hoc test was performed. $P < 0.05$ was considered statistically significant. Some parametric tests were performed without the test for normality because data distribution was assumed to be normal.

Online supplemental material

Fig. S1 shows a characterization of human keratinocyte colonies. Fig. S2 shows cell division patterns in human keratinocyte colonies. Fig. S3 shows modeling of human keratinocyte behavior in culture. Fig. S4 shows preparation of skin wound samples from young and aged mice. Fig. S5 shows expression analysis of COL17A1 and its associated molecules. Data S1 contains the colony growth Fortran program.

Acknowledgments

We thank Japan Tissue Engineering Co., Ltd. (Ganagori, Japan) for providing the 3T3-J2 cells.

This work was supported by the Japan Society for the Promotion of Science KAKENHI grants (26461660 and 17K102319); by a Grant-in-Aid for Scientific Research on Innovative Areas of the Ministry of Education, Culture, Sports, Science and Technology, Japan (17H05997 and 19H04954); by a Takeda Science Foundation grant to D. Nanba; and by a project for Elucidating and Controlling Mechanisms of Aging and Longevity of the Japan Agency for Medical Research and Development (JP17gm5010002, JP18gm5010002, JP19gm5010002, and JP20gm5010002) to E.K. Nishimura.

The authors declare no competing financial interests.

Author contributions: D. Nanba and E.K. Nishimura conceived the project. F. Toki and D. Nanba performed cell culture experiments and data analysis. K. Asakawa and D. Nanba performed wound healing experiments. H. Matsumura established the shRNA-expressing HaCaT cell lines and performed the directed migration assay with D. Nanba. H. Toki and D. Nanba developed the program and performed the simulation experiments. K. Shiraishi, K. Sayama, and K. Matsuzaki prepared human skin samples and keratinocytes. D. Nanba and E.K. Nishimura wrote the manuscript.

Submitted: 14 December 2020
Revised: 25 June 2021
Accepted: 12 August 2021

References

Aragona, M., S. Dekoninck, S. Rulands, S. Lenglez, G. Mascré, B.D. Simons, and C. Blanpain. 2017. Defining stem cell dynamics and migration during wound healing in mouse skin epidermis. *Nat. Commun.* 8:14684. https://doi.org/10.1038/ncomms14684

Ashcroft, G.S., S.J. Mills, and J.J. Ashworth. 2002. Ageing and wound healing. *Biogerontology*. 3:337–345. https://doi.org/10.1023/A:1021399228395

Banks-Schlegel, S., and H. Green. 1980. Formation of epidermis by serially cultivated human epidermal cells transplanted as an epithelium to athymic mice. *Transplantation*. 29:308–313. https://doi.org/10.1097/00007890-198004000-00010

Barrandon, Y., and H. Green. 1987a. Cell migration is essential for sustained growth of keratinocyte colonies: the roles of transforming growth factor-alpha and epidermal growth factor. *Cell*. 50:1131–1137. https://doi.org/10.1016/0092-8674(87)90179-6

Barrandon, Y., and H. Green. 1987b. Three clonal types of keratinocyte with different capacities for multiplication. *Proc. Natl. Acad. Sci. USA*. 84:2302–2306. https://doi.org/10.1073/pnas.84.8.2302

Coulombe, P.A. 2003. Wound epithelialization: accelerating the pace of discovery. *J. Invest. Dermatol.* 121:219–230. https://doi.org/10.1046/j.1523-1747.2003.12387.x

Dover, R., and C.S. Potten. 1988. Heterogeneity and cell cycle analyses from time-lapse studies of human keratinocytes in vitro. *J. Cell Sci.* 89:359–364. https://doi.org/10.1242/jcs.89.3.359

Eming, S.A., P. Martin, and M. Tomic-Canic. 2014. Wound repair and regeneration: mechanisms, signaling, and translation. *Sci. Transl. Med.* 6:265sr6. https://doi.org/10.1126/scitranslmed.3009337

Farinas, A.F., R. Bamba, A.C. Pollins, N.L. Cardwell, L.B. Nanney, and W.P. Thayer. 2018. Burn wounds in the young versus the aged patient display differential immunological responses. *Burns*. 44:1475–1481. https://doi.org/10.1016/j.burns.2018.05.012

Franzke, C.W., K. Tasanen, H. Schäcke, Z. Zhou, K. Tryggvason, C. Mauch, P. Zigrino, S. Sunnarborg, D.C. Lee, F. Fahrenholz, and L. Bruckner-Tuderman. 2002. Transmembrane collagen XVII, an epithelial adhesion protein, is shed from the cell surface by ADAMs. *EMBO J.* 21:5026–5035. https://doi.org/10.1093/emboj/cdf532

Franzke, C.W., L. Bruckner-Tuderman, and C.P. Blobel. 2009. Shedding of collagen XVII/BP180 in skin depends on both ADAM10 and ADAM9. *J. Biol. Chem.* 284:23386–23396. https://doi.org/10.1074/jbc.M109.034090

Green, H., O. Kehinde, and J. Thomas. 1979. Growth of cultured human epidermal cells into multiple epithelia suitable for grafting. *Proc. Natl. Acad. Sci. USA*. 76:5665–5668. https://doi.org/10.1073/pnas.76.11.5665

Gurtner, G.C., S. Werner, Y. Barrandon, and M.T. Longaker. 2008. Wound repair and regeneration. *Nature*. 453:314–321. https://doi.org/10.1038/nature07039

Hamill, K.J., S.B. Hopkinson, M.F. Jonkman, and J.C. Jones. 2011. Type XVII collagen regulates lamellipod stability, cell motility, and signaling to Rac1 by targeting bullous pemphigoid antigen 1e to alpha6beta4 integrin. *J. Biol. Chem.* 286:26768–26780. https://doi.org/10.1074/jbc.M110.203646

Hirako, Y., and K. Owaribe. 1998. Hemidesmosomes and their unique transmembrane protein BP180. *Microsc. Res. Tech.* 43:207–217. https://doi.org/10.1002/(SICI)1097-0029(19981101)43:3<207::AID-JEMT2>3.0.CO;2-Z

Hirose, T., J. Kotoku, F. Toki, E.K. Nishimura, and D. Nanba. 2021. Label-free quality control and identification of human keratinocyte stem cells by deep learning-based automated cell tracking. *Stem Cells*. 39:1091–1100. https://doi.org/10.1002/stem.3371

Hiroyasu, S., Z.T. Colburn, and J.C. Jones. 2016. A hemidesmosomal protein regulates actin dynamics and traction forces in motile keratinocytes. *FASEB J.* 30:2298–2310. https://doi.org/10.1096/fj.201500160R

Hofmann, S.C., U. Voith, V. Schönau, L. Sorokin, L. Bruckner-Tuderman, and C.W. Franzke. 2009. Plasmin plays a role in the in vitro generation of the linear IgA dermatosis antigen LADB97. *J. Invest. Dermatol.* 129:1730–1739. https://doi.org/10.1038/jid.2008.424

Holt, D.R., S.J. Kirk, M.C. Regan, M. Hurson, W.J. Lindblad, and A. Barbul. 1992. Effect of age on wound healing in healthy human beings. *Surgery*. 112:293–297, discussion :297–298.

Hoshikawa, E., T. Sato, Y. Kimori, A. Suzuki, K. Haga, H. Kato, K. Tabeta, D. Nanba, and K. Izumi. 2019. Noninvasive measurement of cell/colony motion using image analysis methods to evaluate the proliferative capacity of oral keratinocytes as a tool for quality control in regenerative medicine. *J. Tissue Eng.* 10:2041731419881528. https://doi.org/10.1177/2041731419881528

Hoshikawa, E., T. Sato, K. Haga, A. Suzuki, R. Kobayashi, K. Tabeta, and K. Izumi. 2021. Cells/colony motion of oral keratinocytes determined by non-invasive and quantitative measurement using optical flow predicts epithelial regenerative capacity. *Sci. Rep.* 11:10403. https://doi.org/10.1038/s41598-021-89073-y

Hynds, R.E., P. Bonfanti, and S.M. Janes. 2018. Regenerating human epithelia with cultured stem cells: feeder cells, organoids and beyond. *EMBO Mol. Med.* 10:139–150. https://doi.org/10.15252/emmm.201708213

Jacków, J., S. Löffek, A. Nyström, L. Bruckner-Tuderman, and C.W. Franzke. 2016a. Collagen XVII Shedding Suppresses Re-Epithelialization by Directing Keratinocyte Migration and Dampening mTOR Signaling. *J. Invest. Dermatol.* 136:1031–1041. https://doi.org/10.1016/j.jid.2016.01.012

Jacków, J., A. Schlosser, R. Sormunen, A. Nyström, C. Sitaru, K. Tasanen, L. Bruckner-Tuderman, and C.W. Franzke. 2016b. Generation of a Functional Non-Shedding Collagen XVII Mouse Model: Relevance of Collagen XVII Shedding in Wound Healing. *J. Invest. Dermatol.* 136:516–525. https://doi.org/10.1016/j.jid.2015.10.060

Keyes, B.E., S. Liu, A. Asare, S. Naik, J. Levorse, L. Polak, C.P. Lu, M. Nikolova, H.A. Pasolli, and E. Fuchs. 2016. Impaired Epidermal to Dendritic T Cell Signaling Slows Wound Repair in Aged Skin. *Cell.* 167:1323–1338.e14. https://doi.org/10.1016/j.cell.2016.10.052

Kim, D.J., T. Mustoe, and R.A. Clark. 2015. Cutaneous wound healing in aging small mammals: a systematic review. *Wound Repair Regen.* 23:318–339. https://doi.org/10.1111/wrr.12290

Kinoshita, K., T. Munesue, F. Toki, M. Isshiki, S. Higashiyama, Y. Barrandon, E.K. Nishimura, Y. Yanagihara, and D. Nanba. 2019. Automated collective motion analysis validates human keratinocyte stem cell cultures. *Sci. Rep.* 9:18725. https://doi.org/10.1038/s41598-019-55279-4

Laval, S., H. Laklai, M. Fanjul, M. Pucelle, H. Laurell, A. Billon-Galés, S. Le Guellec, M.B. Delisle, A. Sonnenberg, C. Susini, et al. 2014. Dual roles of hemidesmosomal proteins in the pancreatic epithelium: the phosphoinositide 3-kinase decides. *Oncogene.* 33:1934–1944. https://doi.org/10.1038/onc.2013.146

Lin, L., T. Betsuyaku, L. Heimbach, N. Li, D. Rubenstein, S.D. Shapiro, L. An, G.J. Giudice, L.A. Diaz, R.M. Senior, and Z. Liu. 2012. Neutrophil elastase cleaves the murine hemidesmosomal protein BP180/type XVII collagen and generates degradation products that modulate experimental bullous pemphigoid. *Matrix Biol.* 31:38–44. https://doi.org/10.1016/j.matbio.2011.09.003

Liu, Z., X. Zhou, S.D. Shapiro, J.M. Shipley, S.S. Twining, L.A. Diaz, R.M. Senior, and Z. Werb. 2000. The serpin alpha1-proteinase inhibitor is a critical substrate for gelatinase B/MMP-9 in vivo. *Cell.* 102:647–655. https://doi.org/10.1016/S0092-8674(00)00087-8

Liu, N., H. Matsumura, T. Kato, S. Ichinose, A. Takada, T. Namiki, K. Asakawa, H. Morinaga, Y. Mohri, A. De Arcangelis, et al. 2019. Stem cell competition orchestrates skin homeostasis and ageing. *Nature.* 568:344–350. https://doi.org/10.1038/s41586-019-1085-7

Löffek, S., T. Hurskainen, J. Jackow, F.C. Sigloch, O. Schilling, K. Tasanen, L. Bruckner-Tuderman, and C.W. Franzke. 2014. Transmembrane collagen XVII modulates integrin dependent keratinocyte migration via PI3K/Rac1 signaling. *PLoS One.* 9:e87263. https://doi.org/10.1371/journal.pone.0087263

López-Otín, C., M.A. Blasco, L. Partridge, M. Serrano, and G. Kroemer. 2013. The hallmarks of aging. *Cell.* 153:1194–1217. https://doi.org/10.1016/j.cell.2013.05.039

Mazzalupo, S., M.J. Wawersik, and P.A. Coulombe. 2002. An ex vivo assay to assess the potential of skin keratinocytes for wound epithelialization. *J. Invest. Dermatol.* 118:866–870. https://doi.org/10.1046/j.1523-1747.2002.01736.x

Moch, M., R. Windoffer, N. Schwarz, R. Pohl, A. Omenzetter, U. Schnakenberg, F. Herb, K. Chaisaowong, D. Merhof, L. Ramms, et al. 2016. Effects of Plectin Depletion on Keratin Network Dynamics and Organization. *PLoS One.* 11:e0149106. https://doi.org/10.1371/journal.pone.0149106

Murphy, G. 2011. Tissue inhibitors of metalloproteinases. *Genome Biol.* 12:233. https://doi.org/10.1186/gb-2011-12-11-233

Nanba, D. 2019. Human keratinocyte stem cells: From cell biology to cell therapy. *J. Dermatol. Sci.* 96:66–72. https://doi.org/10.1016/j.jdermsci.2019.10.002

Nanba, D., N. Matsushita, F. Toki, and S. Higashiyama. 2013a. Efficient expansion of human keratinocyte stem/progenitor cells carrying a transgene with lentiviral vector. *Stem Cell Res. Ther.* 4:127. https://doi.org/10.1186/scrt338

Nanba, D., F. Toki, N. Matsushita, S. Matsushita, S. Higashiyama, and Y. Barrandon. 2013b. Actin filament dynamics impacts keratinocyte stem cell maintenance. *EMBO Mol. Med.* 5:640–653. https://doi.org/10.1002/emmm.201201839

Nanba, D., F. Toki, S. Tate, M. Imai, N. Matsushita, K. Shiraishi, K. Sayama, H. Toki, S. Higashiyama, and Y. Barrandon. 2015. Cell motion predicts human epidermal stemness. *J. Cell Biol.* 209:305–315. https://doi.org/10.1083/jcb.201409024

Natsuga, K., W. Nishie, M. Nishimura, S. Shinkuma, M. Watanabe, K. Izumi, H. Nakamura, Y. Hirako, and H. Shimizu. 2017. Loss of interaction between plectin and type XVII collagen results in epidermolysis bullosa simplex. *Hum. Mutat.* 38:1666–1670. https://doi.org/10.1002/humu.23344

Nishie, W. 2020. Collagen XVII Processing and Blistering Skin Diseases. *Acta Derm. Venereol.* 100:adv00054–adv00107. https://doi.org/10.2340/00015555-3399

Nishimura, M., W. Nishie, Y. Shirafuji, S. Shinkuma, K. Natsuga, H. Nakamura, D. Sawamura, K. Iwatsuki, and H. Shimizu. 2016. Extracellular cleavage of collagen XVII is essential for correct cutaneous basement membrane formation. *Hum. Mol. Genet.* 25:328–339. https://doi.org/10.1093/hmg/ddv478

Park, S., D.G. Gonzalez, B. Guirao, J.D. Boucher, K. Cockburn, E.D. Marsh, K.R. Mesa, S. Brown, P. Rompolas, A.M. Haberman, et al. 2017. Tissue-scale coordination of cellular behaviour promotes epidermal wound repair in live mice. *Nat. Cell Biol.* 19:155–163. https://doi.org/10.1038/ncb3472

Peking, P., U. Koller, and E.M. Murauer. 2018. Functional therapies for cutaneous wound repair in epidermolysis bullosa. *Adv. Drug Deliv. Rev.* 129:330–343. https://doi.org/10.1016/j.addr.2017.12.003

Rheinwald, J.G., and H. Green. 1975. Serial cultivation of strains of human epidermal keratinocytes: the formation of keratinizing colonies from single cells. *Cell.* 6:331–343. https://doi.org/10.1016/S0092-8674(75)80001-8

Rochat, A., K. Kobayashi, and Y. Barrandon. 1994. Location of stem cells of human hair follicles by clonal analysis. *Cell.* 76:1063–1073. https://doi.org/10.1016/0092-8674(94)90383-2

Rochat, A., N. Grasset, F. Gorostidi, S. Lathion, and Y. Barrandon. 2012. Regeneration of epidermis from adult human keratinocyte stem cells. *In* Handbook of Stem Cells. Vol. 2. A. Atala, and R. Lanza, editors. Academic Press, London. 767–780.

Rørth, P. 2009. Collective cell migration. *Annu. Rev. Cell Dev. Biol.* 25:407–429. https://doi.org/10.1146/annurev.cellbio.042308.113231

Roshan, A., K. Murai, J. Fowler, B.D. Simons, V. Nikolaidou-Neokosmidou, and P.H. Jones. 2016. Human keratinocytes have two interconvertible modes of proliferation. *Nat. Cell Biol.* 18:145–156. https://doi.org/10.1038/ncb3282

Schindelin, J., I. Arganda-Carreras, E. Frise, V. Kaynig, M. Longair, T. Pietzsch, S. Preibisch, C. Rueden, S. Saalfeld, B. Schmid, et al. 2012. Fiji: an open-source platform for biological-image analysis. *Nat. Methods.* 9:676–682. https://doi.org/10.1038/nmeth.2019

Sgonc, R., and J. Gruber. 2013. Age-related aspects of cutaneous wound healing: a mini-review. *Gerontology.* 59:159–164. https://doi.org/10.1159/000342344

Shurin, G.V., Z.R. Yurkovetsky, G.S. Chatta, I.L. Tourkova, M.R. Shurin, and A.E. Lokshin. 2007. Dynamic alteration of soluble serum biomarkers in healthy aging. *Cytokine.* 39:123–129. https://doi.org/10.1016/j.cyto.2007.06.006

Ståhle-Bäckdahl, M., M. Inoue, G.J. Guidice, and W.C. Parks. 1994. 92-kD gelatinase is produced by eosinophils at the site of blister formation in bullous pemphigoid and cleaves the extracellular domain of recombinant 180-kD bullous pemphigoid autoantigen. *J. Clin. Invest.* 93:2022–2030. https://doi.org/10.1172/JCI117196

Sun, T.T., and H. Green. 1976. Differentiation of the epidermal keratinocyte in cell culture: formation of the cornified envelope. *Cell.* 9:511–521. https://doi.org/10.1016/0092-8674(76)90033-7

Sun, B.K., Z. Siprashvili, and P.A. Khavari. 2014. Advances in skin grafting and treatment of cutaneous wounds. *Science.* 346:941–945. https://doi.org/10.1126/science.1253836

Tasanen, K., L. Tunggal, G. Chometon, L. Bruckner-Tuderman, and M. Aumailley. 2004. Keratinocytes from patients lacking collagen XVII display a migratory phenotype. *Am. J. Pathol.* 164:2027–2038. https://doi.org/10.1016/S0002-9440(10)63762-5

Tate, S., M. Imai, N. Matsushita, E.K. Nishimura, S. Higashiyama, and D. Nanba. 2015. Rotation is the primary motion of paired human epidermal

keratinocytes. *J. Dermatol. Sci.* 79:194–202. https://doi.org/10.1016/j.jdermsci.2015.05.008

Toki, F., D. Nanba, E.K. Nishimura, and K. Matsuzaki. 2020. Evaluation of the proliferative potential of skin keratinocytes and fibroblasts isolated from critical limb ischemia patients. *Regen. Ther.* 14:222–226. https://doi.org/10.1016/j.reth.2020.03.016

Tsuruta, D., T. Hashimoto, K.J. Hamill, and J.C. Jones. 2011. Hemidesmosomes and focal contact proteins: functions and cross-talk in keratinocytes, bullous diseases and wound healing. *J. Dermatol. Sci.* 62:1–7. https://doi.org/10.1016/j.jdermsci.2011.01.005

Uchihashi, M., Y. Hirata, T. Fujita, and S. Matsukura. 1982. Age-related decrease of urinary excretion of human epidermal growth factor (hEGF). *Life Sci.* 31:679–683. https://doi.org/10.1016/0024-3205(82)90769-X

Usui, M.L., R.A. Underwood, J.N. Mansbridge, L.A. Muffley, W.G. Carter, and J.E. Olerud. 2005. Morphological evidence for the role of suprabasal keratinocytes in wound reepithelialization. *Wound Repair Regen.* 13:468–479. https://doi.org/10.1111/j.1067-1927.2005.00067.x

van Bodegraven, E.J., and S. Etienne-Manneville. 2020. Intermediate filaments against actomyosin: the david and goliath of cell migration. *Curr. Opin. Cell Biol.* 66:79–88. https://doi.org/10.1016/j.ceb.2020.05.006

Verraes, S., W. Hornebeck, M. Polette, L. Borradori, and P. Bernard. 2001. Respective contribution of neutrophil elastase and matrix metalloproteinase 9 in the degradation of BP180 (type XVII collagen) in human bullous pemphigoid. *J. Invest. Dermatol.* 117:1091–1096. https://doi.org/10.1046/j.0022-202x.2001.01521.x

Yang, Q., Y. Zhang, H. Yin, and Y. Lu. 2020. Topical Recombinant Human Epidermal Growth Factor for Diabetic Foot Ulcers: A Meta-Analysis of Randomized Controlled Clinical Trials. *Ann. Vasc. Surg.* 62:442–451. https://doi.org/10.1016/j.avsg.2019.05.041

JCB

Supplemental material

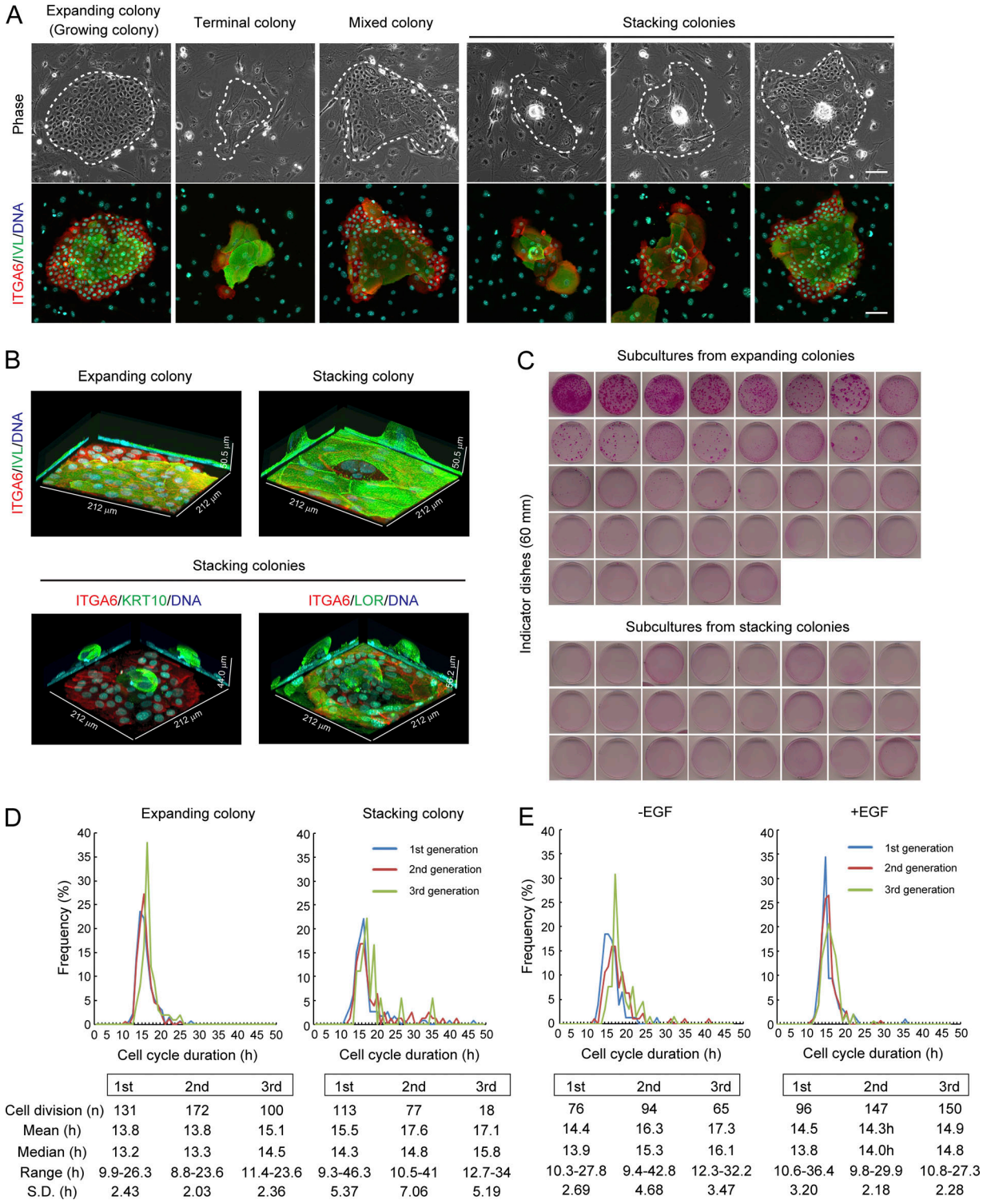

	Expanding colony			Stacking colony		
	1st	2nd	3rd	1st	2nd	3rd
Cell division (n)	131	172	100	113	77	18
Mean (h)	13.8	13.8	15.1	15.5	17.6	17.1
Median (h)	13.2	13.3	14.5	14.3	14.8	15.8
Range (h)	9.9-26.3	8.8-23.6	11.4-23.6	9.3-46.3	10.5-41	12.7-34
S.D. (h)	2.43	2.03	2.36	5.37	7.06	5.19

	-EGF			+EGF		
	1st	2nd	3rd	1st	2nd	3rd
Cell division (n)	76	94	65	96	147	150
Mean (h)	14.4	16.3	17.3	14.5	14.3h	14.9
Median (h)	13.9	15.3	16.1	13.8	14.0h	14.8
Range (h)	10.3-27.8	9.4-42.8	12.3-32.2	10.6-36.4	9.8-29.9	10.8-27.3
S.D. (h)	2.69	4.68	3.47	3.20	2.18	2.28

Figure S1. **Characterization of human keratinocyte colonies. (A)** Appearance of several colony types of human epidermal keratinocytes 6 d after inoculation in phase-contrast (upper) and immunofluorescence (lower) images with ITGA6 and IVL antibodies. Scale bars, 100 µm. Images of expanding and stacking colonies are also represented in Fig. 1 C. **(B)** 3D reconstruction of expanding and stacking colonies on culture day 6. Keratinocyte colonies were immunostained with ITGA6 and IVL antibodies. Stacking colonies were also immunostained with keratin 10 (KRT10) and loricrin (LOR) antibodies. **(C)** Subcloning and further expansion of single expanding and stacking colonies into new 60-mm cell culture dishes using cloning rings. 37 expanding and 24 stacking colonies were analyzed. **(D)** Distribution of cell cycle duration in each cell generation during the formation of expanding and stacking colonies. The data shown were obtained from 403 cell divisions in 6 expanding colony formations and from 208 cell divisions in 9 stacking colony formations. **(E)** Distribution of cell cycle duration in each cell generation during keratinocyte colony formation with and without EGF. The data shown were obtained from 235 cell divisions in six colonies and from 393 cell divisions in seven colonies in −EGF and +EGF conditions, respectively.

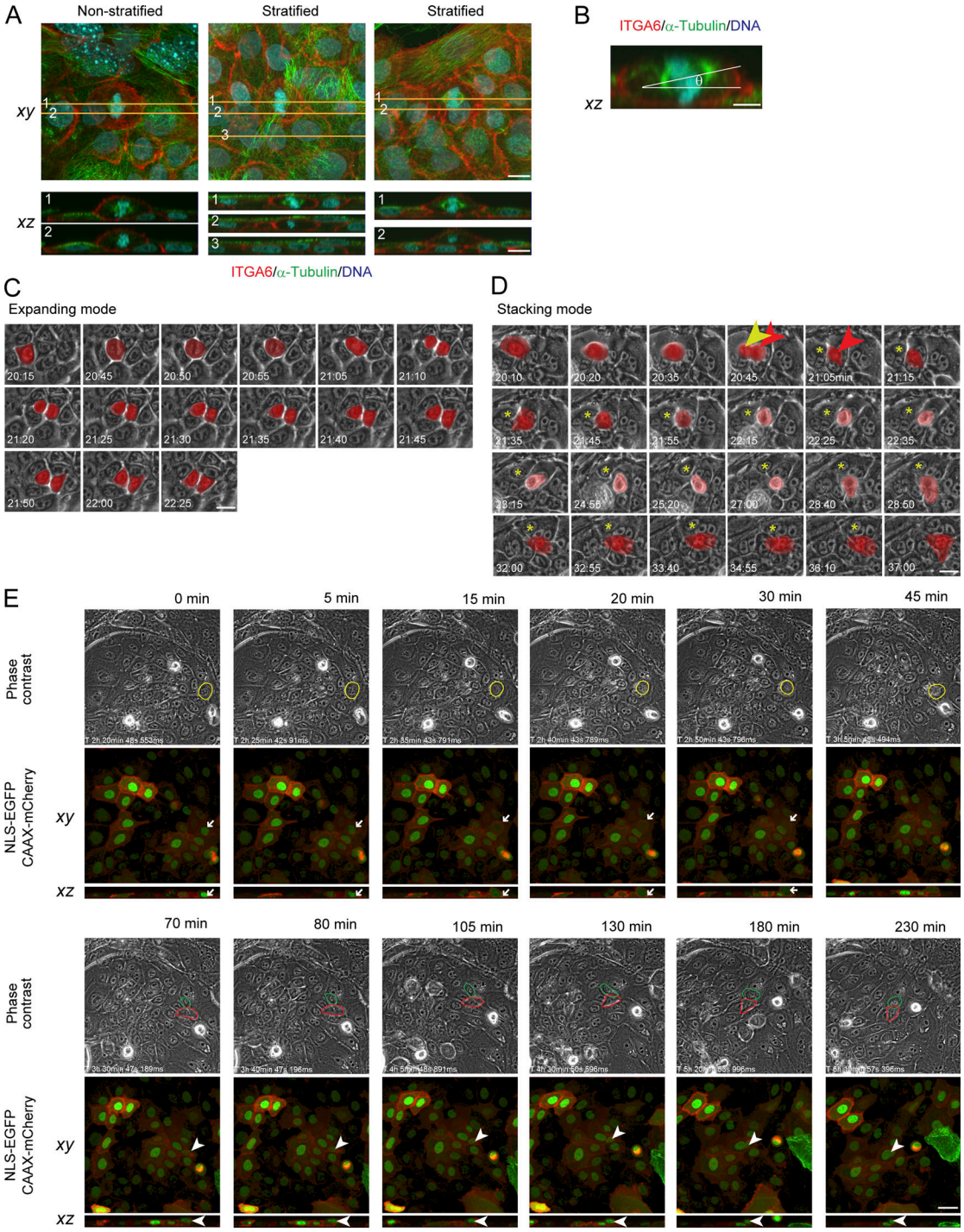

Figure S2. **Cell division patterns in human keratinocyte colonies. (A)** Upper and lower images show representative horizontal (*xy*) and vertical (*xz*) sections of dividing keratinocytes during colony formation. Nonstratified (culture day 4) and stratified (culture day 6) colonies and keratinocyte sheets (culture day 15) were analyzed. Cells were immunostained with anti-ITGA6 and anti-α-tubulin. Lines (orange) in horizontal sections indicate their corresponding vertical sections. Scale bars, 10 µm. **(B)** Schematic representation of measurement of cell division angles. The angle of the cell division axis in a dividing keratinocyte was defined as an acute crossed-axes angle ($0 \leq \theta \leq \pi/2$) between a line linking two centrosomes and the basal plane. Scale bar, 5 µm. **(C)** Detailed presentation of the expanding mode of cell behavior after cell division, as described for Fig. 2 F. Nuclei are labeled with a pseudo-color (red). Scale bar, 20 µm. **(D)** Detailed presentation of the stacking mode of cell behavior after cell division, as described for Fig. 2 F. Nuclei are labeled with a pseudo-color (red). The yellow arrowhead indicates one of the dividing nuclei. A daughter cell containing this nucleus resides at the basal layer (yellow asterisks). Red arrowheads indicate another daughter cell that remains in the suprabasal layer after cell division. Scale bar, 20 µm. **(E)** Confirmation of stacking mode of cell behavior after cell division. The vertical movements of keratinocytes in the stacking mode were confirmed by confocal microscopy of keratinocytes expressing nuclear-targeted GFP and plasma membrane–targeted mCherry. The cell surrounded with a yellow circle gave rise to two daughter cells surrounded by green and red circles in phase-contrast images. White arrows and arrowheads in horizontal (*xy*) and vertical (*xz*) sections obtained by confocal microscopy indicate cells surrounded by yellow and red circles in phase-contrast images. Scale bar, 50 µm.

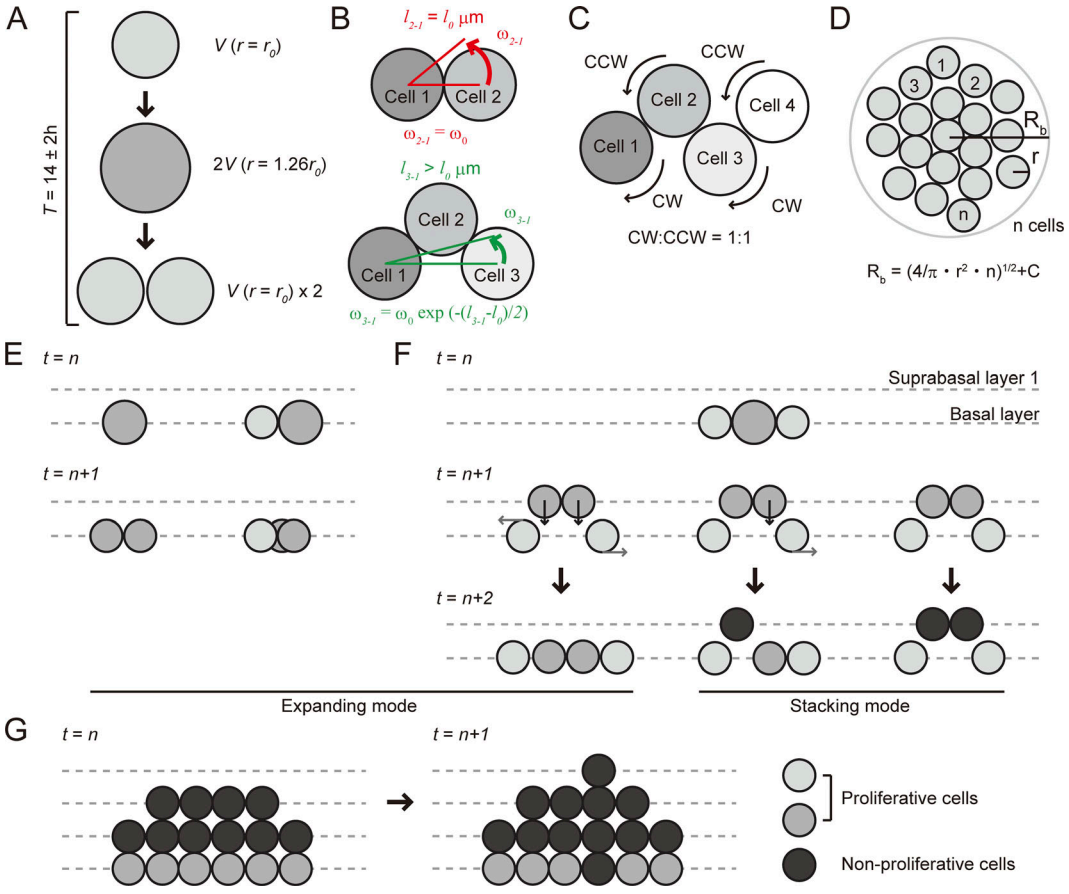

Figure S3. **Modeling of human keratinocyte behavior in culture. (A)** Keratinocytes grow and then divide every 14 ± 2 h (68.9% of divisions occurred within this period in our culture condition) as observed in Fig. 1 J. **(B)** The rotational speed of cell *j* against cell *i*, ω_{j-i}, is defined as $\omega_{j-i} = \omega_0 \exp[-(l_{j-i}-l_0)/2]$. l_{j-i} is the distance between the centers of cell *i* and cell *j*. **(C)** The rotational motion in two-cell colonies of human keratinocytes has two directions; clockwise (CW) and counterclockwise (CCW). The ratio of CW to CCW rotation is defined as 1:1 in this model. **(D)** The boundary that limits cell locomotion during colony formation is placed in this model. The radius of the boundary of a colony is defined as $R_b = (4/\pi \cdot r^2 \cdot n)^{1/2} + C$. **(E)** When basal cells are not totally surrounded by other basal cells, they divide horizontally in the basal layer where cells do not exist. **(F)** When basal cells are entirely surrounded by neighboring basal cells, cell division occurs in the suprabasal layer. If neighboring basal cells move and create a space for the divided cells in the basal layer, the daughter cells can reside in the basal layer, as shown on the left. When there is no space in the basal layer, the daughter cells remain in the suprabasal layer where cells cannot divide, as shown on the middle and right. **(G)** All basal cells can continuously divide, but a basal cell stops proliferating when it has more than three cells on it.

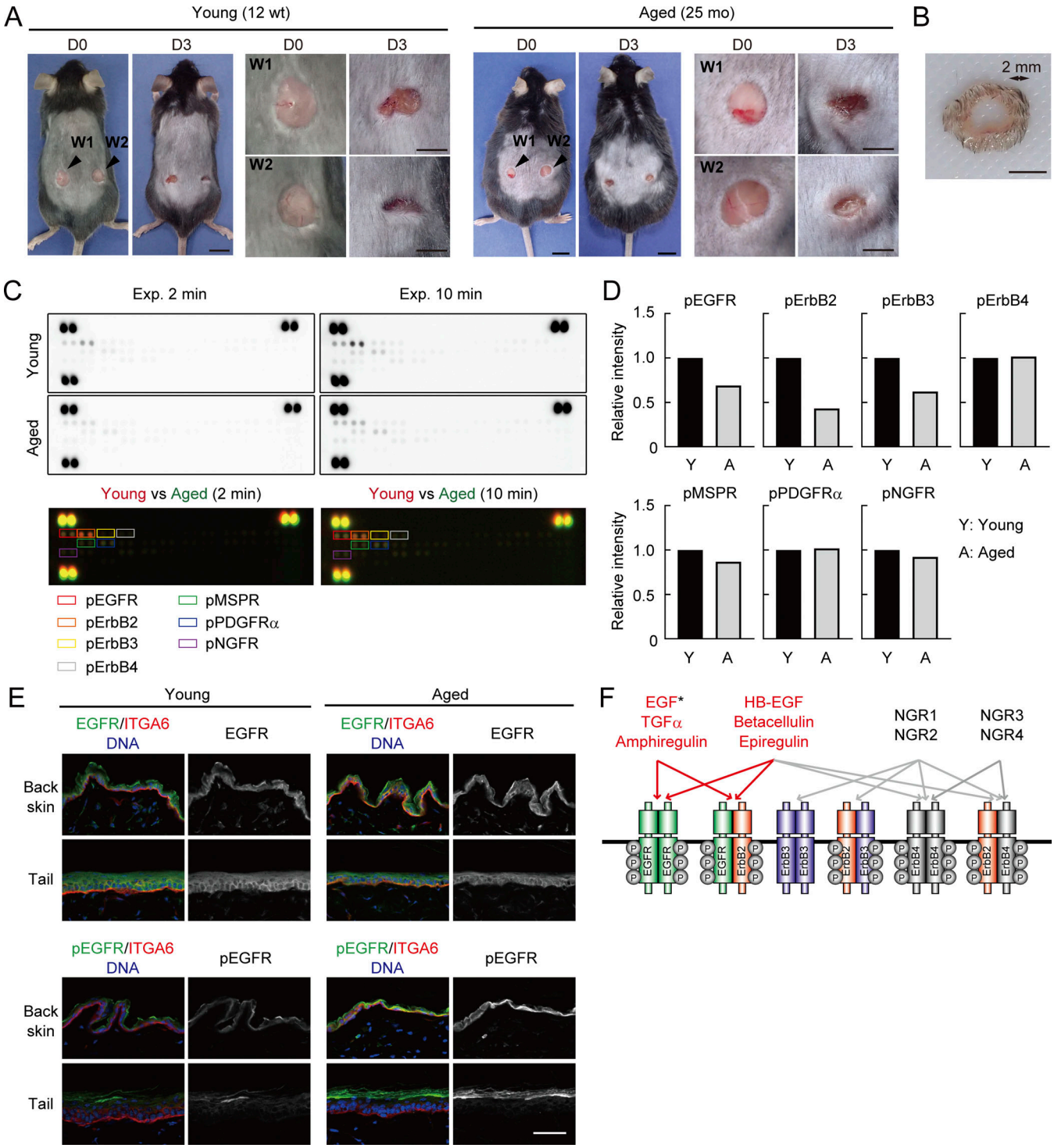

Figure S4. **Preparation of skin wound samples from young and aged mice. (A)** Wounds were created in the shaved dorsal skin of young (left) and aged right) mice, as indicated by arrowheads. 3 d after wounding, the mice were euthanized, and their skin was isolated for analysis. Images are representative of three independent experiments. Scale bars, 1 cm (left); 0.5 cm (right). **(B)** A representative image of skin wound samples. Approximately 2-mm margins of the wound were homogenized and lysed for protein extraction. Scale bar, 0.5 cm. **(C)** Images of mouse phospho-RTK arrays using protein lysates extracted from skin wounds of young and aged mice. The left and right columns show membranes detected with short and long exposure times, respectively. Black and white images obtained from young and aged mice were converted into color images, and merged color images were then generated to identify signals that show age-associated changes. Red and green spots indicate signals from young and aged mice, respectively. **(D)** Quantification of the signal intensity of several phospho-RTK spots. The values were averages of two independent spots for each phospho-RTK. **(E)** Distribution of EGFR and phosphorylated EGFR (pEGFR) in normal skin isolated from young and aged mice. Dorsal and tail skin was examined. Skin samples were also immunostained with anti-ITGA6 to visualize basal cells in the epidermis. Scale bar, 50 µm. **(F)** Schematic representation of the network of ErbB and EGF family molecules. EGF family growth factors bind to their specific receptors formed by the dimerization of ErbB molecules. EGFR ligands are the potential targets for age-associated decline of EGFR signaling. *, EGF was used to activate EGFR in this study.

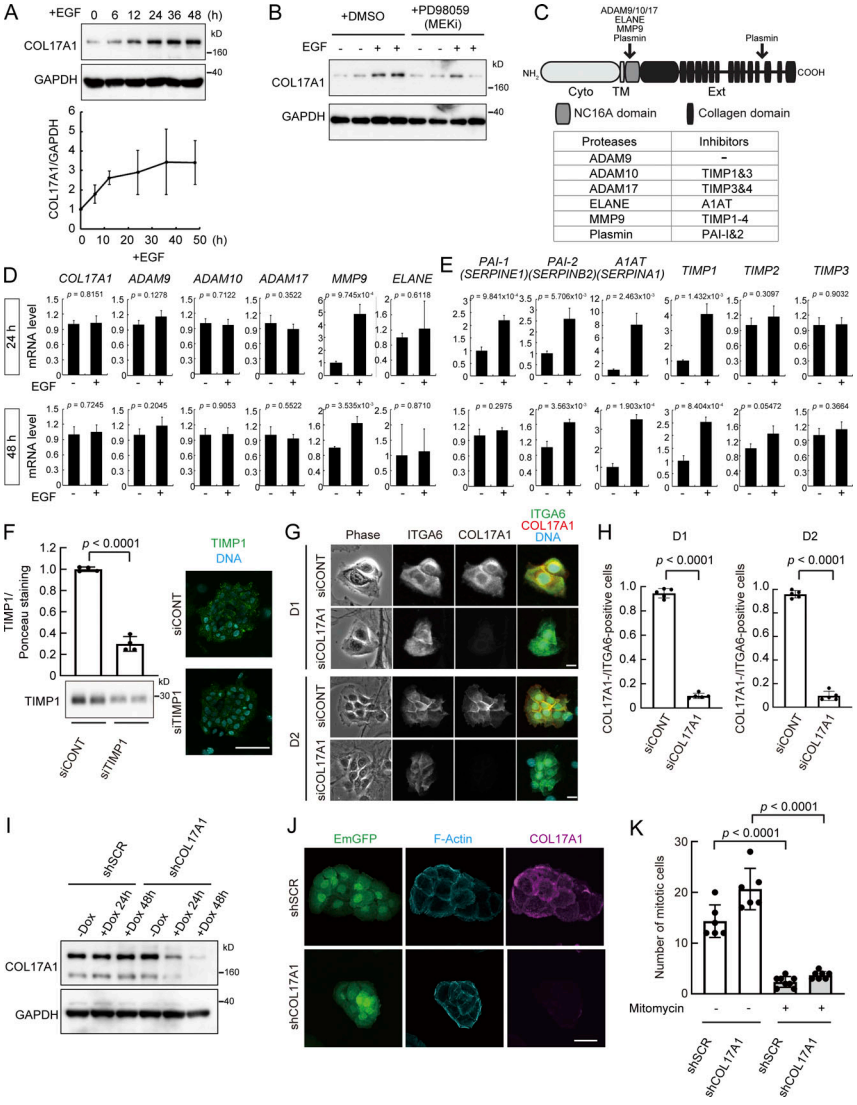

Figure S5. **Expression analysis of COL17A1 and its associated molecules. (A)** Time-course analysis of COL17A1 expression. Keratinocytes were grown in complete growth medium for 7 d and then further incubated in basal medium for 24 h before EGF stimulation. Keratinocytes were harvested at different time points after EGF stimulation, as indicated, and the expression of COL17A1 was analyzed by Western blotting. GAPDH expression was used as a loading control. The Western blotting image is representative of triplicate experiments. The values (mean ± SD) were obtained from three loadings prepared from a single experiment. **(B)** Expression of COL17A1 in human keratinocytes treated with and without 10 nM EGF and 20 µM of the MEK inhibitor PD98059. The Western blotting image is representative of duplicate experiments. GAPDH expression was used as a loading control. **(C)** Upper panel: Schematic representation of the COL17A1 structure containing cytoplasmic (Cyto), transmembrane (TM), and extracellular (Ext) domains, and its protease cleavage sites. The molecular structure of COL17A1 is modified from Hirako and Owaribe (1998). Lower panel: Proteases and their inhibitors. **(D)** mRNA expression levels of *COL17A1* and its associated proteases, including *ADAM9*, *ADAM10*, *ADAM17*, *MMP9*, and *ELANE*. Keratinocytes were grown in complete growth medium for 7 d and then further incubated in basal medium for 24 h before EGF stimulation. Keratinocytes were harvested after 24 and 48 h of EGFR activation. mRNA expression levels were analyzed by quantitative PCR. The values indicate mean ± SD obtained from triplicate experiments. **(E)** mRNA expression levels of COL17A1-associated natural protease inhibitors, including *PAI-I (SERPINE1)*, *PAI-2 (SERPINB2)*, *A1AT (SERPINA1)*, *TIMP1*, *TIMP2*, and *TIMP3*, were also analyzed by quantitative PCR. **(F)** Secretion of TIMP1 into the culture medium from keratinocytes treated with control siRNA or *TIMP1*-targeting siRNA. TIMP1 secretion was normalized with the intensity of Ponceau staining of protein-transferred membranes. The Western blotting image is representative of duplicate experiments, and the values (mean ± SD) were obtained from four independent loadings prepared from single experiments. siRNA-treated colonies were also immunostained with anti-TIMP1. Scale bar, 100 µm. **(G)** Immunofluorescence images of keratinocytes with anti-COL17A1 and anti-ITGA6. on culture days 1 and 2. Scale bars, 20 µm. **(H)** The ratio of COL17A1-positive cells among ITGA6-positive cells on culture days 1 and 2. The values (mean ± SD) were obtained from 621 and 625 keratinocytes forming 2-cell colonies treated with control siRNA or *COL17A1*-targeting siRNA, respectively, on culture day 1, and from 733 and 490 keratinocytes in colonies treated with control siRNA and *COL17A1*-targeting siRNA, respectively, on culture day 2. **(I)** Western blot analysis of the expression of COL17A1 in HaCaT cells expressing SCR shRNA or *COL17A1*-targeting shRNA. These shRNAs were induced by treatment with Dox. COL17A1 expression was analyzed by Western blotting after treatment with Dox for 24 and 48 h. GAPDH expression was used as a loading control. The Western blotting image is representative of duplicate experiments. **(J)** Representative fluorescent images of HaCaT cells expressing SCR shRNA or *COL17A1*-targeting shRNA. shRNA induction and *COL17A1* knockdown were confirmed by EmGFP expression and immunostaining with anti-COL17A1. Scale bar, 50 µm. **(K)** Inhibition of HaCaT proliferation by treatment with 0.4 µg/ml mitomycin C for 2 h. Mitotic cells were identified by nuclear staining with Hoechst 33342. The values (mean ± SD) were obtained from four independent microscopic areas prepared from a single experiment. P values were calculated with the two-tailed Student's *t* test in D–F, H, and K.

A supplemental dataset, Data S1, that contains the colony growth Fortran program is available online.